

Daniil Perfilev

METHODOLOGY FOR WIND TURBINE BLADE GEOMETRY OPTIMIZATION

Thesis for the degree of Doctor of Science (Technology) to be presented with due permission for public examination and criticism in the Auditorium 1383 at Lappeenranta University of Technology, Lappeenranta, Finland, on the 15th of November, 2013, at noon.

Acta Universitatis
Lappeenrantaensis 542

Supervisor Professor Jari Backman
Laboratory of Fluid Dynamics
LUT Energy
Lappeenranta University of Technology
Finland

Reviewers PhD Grant Laidlaw Ingram
School of Engineering and Computing Sciences
Durham University
Great Britain

PhD Alois Peter Schaffarczyk
Mechanical Engineering Department
Kiel University of Applied Sciences
Germany

Opponent PhD Grant Laidlaw Ingram
School of Engineering and Computing Sciences
Durham University
Great Britain

ISBN 978-952-265-489-2
ISBN 978-952-265-490-8 (PDF)
ISSN-L 1456-4491
ISSN 1456-4491
Lappeenrannan teknillinen yliopisto
Yliopistopaino 2013

Abstract

Daniil Perfiliev

Methodology for wind turbine blade geometry optimization

Lappeenranta 2013

97 pages

Acta Universitatis Lappeenrantaensis 542

Diss. Lappeenranta University of Technology

ISBN 978-952-265-489-2, ISBN 978-952-265-490-8 (PDF),

ISSN-L 1456-4491, ISSN 1456-4491

Nowadays, the upwind three bladed horizontal axis wind turbine is the leading player on the market. It has been found to be the best industrial compromise in the range of different turbine constructions. The current wind industry innovation is conducted in the development of individual turbine components.

The blade constitutes 20-25% of the overall turbine budget. Its optimal operation in particular local economic and wind conditions is worth investigating. The blade geometry, namely the chord, twist and airfoil type distributions along the span, responds to the output measures of the blade performance. Therefore, the optimal wind blade geometry can improve the overall turbine performance.

The objectives of the dissertation are focused on the development of a methodology and specific tool for the investigation of possible existing wind blade geometry adjustments. The novelty of the methodology presented in the thesis is the multiobjective perspective on wind blade geometry optimization, particularly taking simultaneously into account the local wind conditions and the issue of aerodynamic noise emissions. The presented optimization objective approach has not been investigated previously for the implementation in wind blade design.

The possibilities to use different theories for the analysis and search procedures are investigated and sufficient arguments derived for the usage of proposed theories. The tool is used for the test optimization of a particular wind turbine blade. The sensitivity analysis shows the dependence of the outputs on the provided inputs, as well as its relative and absolute divergences and instabilities. The pros and cons of the proposed technique are seen from the practical implementation, which is documented in the results, analysis and conclusion sections.

Keywords: wind turbine, blade geometry, optimization, desirability function, differential evolution algorithm

UDC: 621.548:519.85:004.94

Acknowledgements

The research work has been carried out in the Laboratory of Fluid Dynamics of Lappeenranta University of Technology (LUT) during years 2010-2013. It received funding from the university budget and the European Regional Development Fund (ERDF) under RENETECH project aimed to enhance the wind energy sector in South-Carelian region of Finland.

I would like to express my deepest gratitude to my supervisor Professor Jari Backman, who put a lot of efforts during these years and helped me in managing scientific and organizational problems. In any situation he was invariably encouraging me and had the ability to show any circumstance in a positive way.

I thank the members of the steering group Professor Jari Hämäläinen and Professor Heikki Haario who organized regular seminars and discussions where I could share my ideas and receive objective feedback.

Special thanks go to my examiners Dr. Grant Ingram and Dr. Alois Schaffarczyk for deep and constructive comments on the preliminary text of the thesis. Their comments helped me to improve the monograph style as well as to add a valuable feature to the methodology functionality.

Also I would like to thank Michael Zaaijer from Delft University of Technology for deep and extensive review of the paper for EWEA conference, which finally positioned my work in the current track.

Thanks go to my colleague from LUT MSc. Anna Kosmacheva for cooperative work under article publication.

The very big “Thank you” goes to our faculty secretary Piipa Virkki for been superfast, super-effective and super-easy woman. Wish there would be more people like she, it would be easier and nicer to live for all of us.

The additional thanks go to Sari Silventoinen for her talent, patience and accurateness during the proofreading of the monograph and several of my publications.

Also I express my gratitude to Peter Jones, who taught us how to present ideas and gave valuable comments during the proofreading of my journal article.

Finally, thanks go to my family, wife and friends from here and Russia. This work is dedicated to them, as these people constitute the meaning of my life.

Daniil Perfilev
October 2013
Lappeenranta, Finland

Contents

Abstract

Acknowledgements

Contents

List of publications	9
Nomenclature	11
1 Introduction	15
1.1 Wind energy overview	15
1.2 Literature review on the problem of blade shape optimization.....	17
1.3 Objectives and overview of the thesis.....	20
2 Analysis blocks	23
2.1 Aerodynamics.....	23
2.1.1 Lift and drag characteristics	27
2.1.2 Aerodynamic power coefficient, forces and moments.....	30
2.2 Mechanics.....	32
2.2.1 Structural properties of the blade cross-section	33
2.2.2 The static beam theory for wind turbine blade	39
2.3 Economics	41
2.4 Aerodynamic noise model.....	43
2.4.1 Turbulent inflow noise	45
2.4.2 Trailing edge noise.....	47
3 Optimization tools	49
3.1 Desirability function approach for decision making	49
3.1.1 Classification of multiobjective methods.....	49
3.1.2 Desirability function	50
3.2 Differential evolution algorithm (DEA).....	53
3.2.1 Differential evolution strategies.....	55
4 Initial information of the case study	57
4.1 WindPACT 1.5 MW wind turbine	57
4.2 Chord, twist and airfoil distribution boundaries.....	59
5 Methodology results	63
5.1 Optimal tip speed ratio and pitch angle.....	63
5.2 Investigation of mechanic structural parameters.....	64
5.3 Convergence capabilities of DEA strategies	67
5.4 Desirability function sensitivity analysis	68

6 Summary and Conclusions	76
6.1 Suggestions for future work	79
References	81
Appendix A: Developed computer application	87
A1. Existing software for wind turbine design	87
A2. General introduction of the developed software	88

List of publications

This monograph contains material from the following papers.

- I. Koivuniemi, A., Perfiliev, D., Heikkinen, J.P., Backman, J., Pyrhonen, O. (2011). Modeling of wind turbine performance in complex terrain using dynamic simulation. In: *Proceedings of the 15th World Multi-conference on Systemics, Cybernetics and Informatics (WMSCI)*, pp. 228-233. Orlando.
- II. Perfiliev, D. and Backman, J. (2013a). Matlab tool for multiobjective wind blade geometry optimization. In: *Proceedings of the European Wind Energy Association conference (EWEA)*. Vienna.
- III. Perfiliev, D., Kosmacheva, A., Backman, J., and Hamalainen, J. (2013a). Semi automated improvement of wind blade design. In: *Proceedings of the 10th European Conference on Turbomachinery Fluid Dynamics and Thermodynamics (ETC10)*. Lappeenranta.
- IV. Perfiliev, D., Hamalainen, J., and Backman, J. (2013b). Robust analyzing tool for wind turbine blades coupled with multiobjective optimization. *Journal of Energy and Power Engineering*. (accepted for publication).
- V. Perfiliev, D. and Backman, J. (2013b). Wind turbine blade geometry optimization with differential evolution algorithm and desirability function approach. *Renewable Energy*. Submitted for publication.

Author's contribution

The author of this doctoral thesis is the principal author and investigator in Publication I. M.Sc. Aapo Koivuniemi and Janne P. Heikkinen were responsible for the composition of the model.

The author of this thesis is the principal author and investigator in Publications II, IV and V. Professor Jari Backman and Professor Jari Hämäläinen were responsible for supervising the work.

The author of this thesis is the principal author and investigator in Publication III. M.Sc. Anna Kosmacheva is responsible for a part of the investigation and result analysis.

The novelty of the methodology presented in the thesis is the multiobjective perspective on wind blade geometry optimization, particularly taking into account local wind conditions and the issue of aerodynamic noise emissions. The presented optimization

objective approach has never been investigated before for the implementation in wind blade design. The developed computer application is a practical implementation of the scientific approach.

Nomenclature

Latin alphabet

a	axial induction factor	
A	area, scale factor	$m^2, m/s$
a'	tangential induction factor	
B	number of blades	
b	fixed rotor cost component	
c	chord	m
C	rotor cost	
C_p	aerodynamic power coefficient	
C_r	crossover probability	
C_{rotor}	relative rotor cost	
D	drag force	N
D	desirability function	
d	objective function code	
E	Youngs modulus	Pa
EA	longitudinal stiffnees	Nm^2
ED	centrifugal stiffness	Nm^2
EI	stiffness inertia	Nm^2
ES	moment of stiffness	Nm^3
f	function	
F	scale factor	
$FVTR$	value to reach	
h	width	m
I	turbulence intensity	
I_D	number of unknown variables	
$I_{itermax}$	maximum considered populations	
I_{NP}	population members	
k	curvature, wave number, shape factor	$1/m$
L	lift force, blade-tower distance, element length, turbulent length scale	N, m
L_w	noise power level	$dB(A)$
M	moment	Nm
m	mass	kg
p	pitch angle, force	deg, N
P	power, perimeter	kW, m

Q	loss correction factor	
r	distance	m
R	blade radius	m
V	wind speed	m/s
S	surface area, Sears function	m ²
SF	safety factor	
t	ply thickness	mm
T	shear force	N
u	linear deflection	m
U	free stream velocity	m/s
w	variable rotor cost component, objective weight	
X	input vector, axis	
x	x coordinate	m
Y	output vector, axis	
y	y coordinate	m
Greek alphabet		
α	flow angle of attack	deg
β	relative flow angle	deg
γ	twist angle, slope of the lift curve	deg, 1/deg
δ	boundary thickness, material thickness	mm
Δ	tip deflection	m
ε	tolerance	
θ	collective angle, angular deformation	deg
λ	tip speed ratio	
μ	viscosity	m ² /s
ρ	density	kg/m ³
σ	solidity, stress	Pa
φ	angle between first principal axis and tip chord	deg
ω	wake rotational speed	rad/s
Ω	blade rotational speed	rad/s
Dimensionless numbers		
M	Mach number	
Re	Reynolds number	

Superscripts

<i>l</i>	unit
*	dimensionless
<i>a</i>	allowable
<i>TE</i>	trailing edge
<i>TI</i>	turbulent inflow
<i>u</i>	ultimate

Subscripts

<i>av</i>	average
<i>c</i>	compression
<i>ch</i>	chord
<i>d</i>	drag
<i>db</i>	double-bias
<i>defl</i>	deflection
<i>i</i>	index
<i>j</i>	index
<i>k</i>	index
<i>l</i>	lift
<i>lin</i>	lining
<i>max</i>	maximum
<i>mid</i>	middle
<i>min</i>	minimum
<i>mut</i>	mutation
<i>n</i>	normal
<i>na</i>	neutral axis
<i>opt</i>	optimum
<i>orig</i>	original
<i>pop</i>	population
<i>rel</i>	relative
<i>t</i>	tangential
<i>t</i>	tensile
<i>te</i>	trailing edge
<i>tot</i>	total
<i>tw</i>	twist
<i>uni</i>	unidirectional

Abbreviations

BEMM	blade element momentum method
CFD	computational fluid dynamics
DE	differential evolution
FEM	finite element method
HAWT	horizontal axis wind turbine
IEC	International Electrotechnical Commission
LFC	low frequency correction
NREL	National Renewable Energy Laboratory
UTRC	United Technologies Research Center

1 Introduction

1.1 Wind energy overview

The first wind energy mentions date back some 2000 years in Persia. The constructions were primitive wood-based vertical-axis wind-catching surfaces. They were used primarily for agricultural purposes: to pump water and to grind grain (Cheremisinoff, 1978). In the seventh century, windmills spread to France and England. In the thirteenth century, they were used almost in all Western European countries.

In the eighteenth century, John Smeaton was the first to discover the wind behaviour rules: linear proportionality of the tip speed, squared proportionality of the maximum torque and cubic proportionality of the maximum power to the incoming wind flow velocity.

The first patent of a wind energy installation is related to the Scottish inventor J. Blyth in 1891 who documented his construction of a vertical axis turbine under patent number GB19401 (Price, 2005). In 1888, the American entrepreneur and inventor C. F. Brush built the first horizontal axis wind turbine with a fully automated control system and rated power of 12 kW. The Danish scientist and inventor Poul la Cour was the first to put an electric generator inside the nacelle of a turbine and succeeded to make it commercially active, building more than 100 turbines in 27 years to produce hydrogen for public lighting systems.

In the nineteenth century, a small wind energy boom occurred in the West of America during the Gold Rush, when fast and small turbines were used for water pumping. However, neither small nor large wind turbine installations have reached the industrial scale because of cheaper coal and diesel engines and big electricity demand which could only be compensated with a centralised electric grid.

The re-emerging of wind energy began somewhere in 1960s in the U.S. and Denmark, as the industry started to face fossil fuel shortcuts (which then led to the first oil crisis in 1973) and publicly recognised the potential danger of nuclear energy. The wind industry continued to develop in Germany and the Netherlands. The market incentives for growth were the feed-in tariff system introduced to support the renewable fuels. Recently, China got involved in the wind industry (approximately from year 2000 on) and has today the world biggest wind capacity installed (over 75 GW by the end of 2012), but is the second after the U.S. in the annual wind power electricity production (Global wind energy council, 2012). To date, however, Denmark has been the leading energy producer from wind on its approximate 35% share of the total energy production of the country (Wind power in Denmark, 2013).

Today, the upwind three bladed horizontal axis wind turbine is the leading player on the market. It has been found to be the best industrial compromise between the range of

different turbine constructions (horizontal and vertical axis of rotation, one-two-three-N bladed, upwind and downwind).

The classical upwind horizontal axis wind turbine consists of the tower, nacelle, hub and blades. The nacelle contains the control and electric equipment: generator, yaw system, pitch control (for pitch regulated turbine), mechanical break, rotation speed and torque control, wind speed and direction control, AC/DC-AC/DC/AC-DC/DC-DC/AC inverter depending on the generator and system type. The shares of the turbine parts in the overall budget of a typical onshore installation in Europe are presented in Table 1.1

Table 1.1: Share of the main components in the overall turbine cost for 5 MW wind turbine (Krohn et al., 2009, p. 37)

Component	Share, %
Tower	26.30
Rotor blades	22.20
Gearbox	12.91
Power converter	5.01
Transformer	3.59
Generator	3.44
Main frame	2.80
Pitch system	2.66
Main shaft	1.91
Rotor hub	1.37
Nacelle housing	1.35
Brake system	1.32
Yaw system	1.25
Rotor bearings	1.22
Screws	1.04
Cables	0.96

The current wind industry innovation is conducted in the development of individual turbine components. The modern horizontal axis turbine efficiency tends to be 45% (Manwell et al., 2009, p. 34) and the budget for onshore installations 1000 euro per kW power (Morthorst, 2009). Even a percent fraction improvement of either the efficiency or budget measures can be considered as a great win and be crucial for the final installation decision making.

The blade constitutes a significant share of the overall turbine budget: about 20–25% according to Table 1.1. Its optimal operation in particular local economic and wind conditions is worth an investigation. The blade geometry, namely the chord, twist and airfoil type distributions along the span, responds to the output measures of the blade

performance. Therefore, the optimal wind blade geometry can improve the overall turbine performance.

1.2 Literature review on the problem of blade shape optimization

The technology development worldwide tends to introduce mathematical descriptions of the phenomena and processes with computer simulation tools instead of conducting heavy and expensive experiments. The roles of fundamental and applied sciences are to find the right theoretical description for the process and program computer software to simulate the process behaviour, which is often coupled with optimization objectives. The preparation of an adequate and reliable model is important.

The analysis and optimization algorithms existing today are able to take into account the wind turbine operation parameters: power production, i.e. power efficiency and wind characteristics, economy measures, noise emissions level and mechanic measures. Although present research works in wind energy optimization assume some of the parameters mentioned above, they do not provide the technique which would consider all the components at once.

Fuglsang, Madsen and Thomsen from the Danish institute RISO have made a thorough research for the optimization problems with respect to wind energy. They recognize three block components in design and optimization procedures (Fuglsang and Madsen, 1999; Fuglsang and Thomsen, 1998). The first one is the initial information block in which the blade designer provides a set of input variables, introduces constraints and preliminary boundaries and defines the objective function. The second component is the calculation. The accepted theory background determines the output parameters of calculation which commonly, for the case of wind turbines, are the design (economic) and operation (technical efficiency, loads, emissions) measures. The third component carries the optimization procedure which makes changes to the wind part design and seeks the best value for the objective function. From the point of the literature review, the most valuable is the theory background for analysis and optimization tools.

The methodology of aerodynamic calculations which are intended for the determination of force and moment distributions along the blade as well as the aerodynamic power coefficient (which shows the efficiency of kinetic wind energy extraction) is based on the classic Blade Element Moment (BEM) method. Being the straightforward linearly applied technique, it is widely used in industrial applications (Laino, 2002; Bossanyi, 2003). The essence of the method with a practical application example has been described by Ingram (2011). However, it requires an extension with the work of Moriarty and Hansen (2005) to include Prandtl hub losses and the Glauert correction due to the increased turbulence level in the far wake, which are both not introduced in the original work of Ingram. A different approach for the aerodynamic flow analysis has been studied by Carcangiu (2008) using the computational fluid dynamics (CFD). Even with the high computer capacities of today, the CFD approach is still not widely applied

in everyday industrial tasks related to optimization, and is often applied as a validation tool for engineering method results (Carcangiu, 2008; Perfiliev et al., 2013b).

The existing wind turbine economy models differ in their complexity with investigations of either one single or several turbine components at once. The turbine components are the blades, nacelle, tower, foundation, electrical equipment for operation and grid connection (if needed). The Levelized Production Cost (LPC) method for the overall wind turbine economy evaluation propagated by Zaaier (2003) is a complex study which involves all major components of the turbine construction and its further operation (including maintenance). It requires large data collections with respect to real values of economic parameters which are usually not revealed by the industry. Therefore, the practical approach tends to eliminate the need for real monetary expressions and to manipulate with dimensionless parameters which can express the current state of the turbine component compared to the chosen reference (or original) state. Xudong et al. (2009) introduce a dimensionless parameter of the relative cost of turbine component in which the turbine component adjustment (which happens during the optimization process) is reflected with the relative change of its cost, relative to the original cost. The work also elaborates on the small fraction of operation and maintenance costs in the summarized capital investments and the possibility to consider the blade structure separately from the rest of turbine components. The dimensionless economy approach with individual blade consideration was used by Fuglsang and Thomsen (1998) as well.

The present thesis investigates and optimizes the aerodynamic noise emission level. The existing theories are divided into CFD based and semi-empirical methods. The CFD based method is presented with the work of Tadamas and Zangeneh (2011) who introduced the hybrid methodology for the calculation of aerodynamic noise sources with Reynolds Averaged Navier-Stokes (RANS) equations and its far-field evolution with Ffowcs Williams-Hawkings approach. The experimental validation of the modelling approach showed good agreement for helicopter and aircraft wings. However, as a CFD based method, the approach requires significant computation efforts and still seeks for simplification in order to be implemented for wind turbine optimization problems. An alternative modelling technique for noise propagation is the semi-empirical approach developed by Brooks et al. (1989) which introduces a straightforward method for empirical calculations based on the flow parameters and blade geometry. The analysis technique was applied by Fuglsang and Madsen (1996) in the optimization of the blade geometry based on noise considerations. The approach of Brooks et al. was carefully studied by Lowson (1993) who stated that among a number of noise sources found by Brooks et al., there are two—trailing edge and inflow noises—which make the most contribution, and it is enough to consider them for a sufficiently accurate calculation result. The statement was partially confirmed by the measurements of Oerlemans et al. (2007), who concluded the dominance of the trailing edge noise in the overall noise spectra.

Indeed, it is tricky to predict and present the noise emission level, particularly because one needs to separate the aerodynamic source from the mechanical one. Absolute majority of the works mentioned above and related to the aerodynamic noise modelling do not give a clear quantification of their method accuracy, concluding on the “good agreement” with experimental data. Only Lawson (1993) derives the reference for the experimental data of Hubbard and Shepherd (NASA, 1984) for the inflow turbulence noise and compares it with the predicted level for a downwind turbine. The relative difference is approximately 0.35%, which is fairly small.

The investigation of mechanic parameters is commonly limited to the introduction of boundary conditions and equations or it determines one of the objective functions. Common international standards of IEC and DS (IEC 61400-1, 2005; DS 412, 1983) are also applied in Finland for the wind blade design, manufacturing and testing. The book of Madsen et al. (1990) recommends the investigation of blade bending moments, rotor tilt and yaw loads, the axial thrust, main shaft torque, as well as bending and torsional moments in the tower. However, the present thesis seeks for objective criteria in the form of equations or inequalities which the wind blade structure has to fulfil. The study of Bir and Migliore (2004) from National Renewable Energy Laboratory (NREL, USA) introduced structural criteria, the ultimate stress and buckling load, which the design blade shall withstand during its lifecycle. Industrial practice adds the criteria of the maximum blade deflection, i.e. static blade-tower clearance, which was covered in the work of Tong (2010, p. 210). The proposed technique considers the static case investigation. On the contrary, an alternative approach was used in the work of Fuglsang and Madsen (1999) in which the dynamic blade fatigue was studied with a non-linear equation coded in «FLEX 4» aeroelastic calculation tool. Hansen (2008) applied the Beam Theory to the wind blade to determine its mechanic structural parameters with respect to the consisting material properties.

From the general point of view, the optimization task highlights two questions: what is the objective function and what is the method of searching the optimal solution.

Fuglsang and Madsen (1999) argue that there are two generations of objective functions which have evolved during the wind energy research history. The first generation includes the maximum annual energy production or maximum turbine efficiency with no constraints on loads. The strength of the first mentioned objective function is that it considers the off-design performance of the turbine while the second one is the primary consideration of the design conditions. The second generation of the objective functions came with the minimum cost of energy, the ratio between the total turbine cost and annual energy production, which is not restricted with the aerodynamic performance. Adequate cost function calculations require the investigation of fatigue and extreme loads and determination of the connection between design loads and budget expenses.

The present thesis introduces the third generation of objective functions, multiobjective ones, which consider several important objectives like the aerodynamic efficiency, turbine cost and noise emission level, and compose the united objective out of the list.

The multiobjective approach has not previously been developed or considered for practical applications. Multiobjective optimization problems arise when two or more objective functions conflict with each other. This is the case for example with the aerodynamic efficiency and turbine cost—the ultimate goal is to maximize the efficiency and minimize the cost. A comprehensive overview of multiobjective optimization techniques was carried out by de Oliveira and Saramago (2010) who introduced the function scalarization (including weight functions), hierarchical approach, trade-off and goal programming methods. Boulet et al. (2009) argue about the pros and cons of the weight function with respect to multiobjective optimization problems and investigate the practical example of optimal spare parts stock management. The work particularly introduces an approach of the desirability weight function developed by Harrington (1965) and Derringer (1994) which has a straightforward way of implementation for the current thesis' problem of blade geometry optimization.

Various optimal search methodologies have been investigated in connection with the wind turbine technology, differing in the rate of convergence, robustness for particular case and CPU time consumption. The work of Fuglsang and Madsen (1999) applies a combination of sequential linear programming and the technique of feasible directions, which is agreed to be robust, although with a slow rate of convergence and big computational effort. A nonlinear optimization of the blade geometry with torque and moment constraints was performed by Xudong et al. (2009), who used the *fmincon* function of Matlab Optimization toolbox. The genetic algorithm as a universal tool was investigated in the wind blade shape optimization problem by Mendez and Greiner (2006). Mendez stressed the optimization for wind turbine application in particular wind conditions which might differ from the standard classes according to the IEC classification (IEC 61400-1, 2005). A comprehensive introduction of differential evolution algorithm with practical examples of engineering applications is presented in the book of Price, Storn and Lampinen (Price et al., 2005).

The current thesis applies the differential evolution algorithm to its all optimization tasks. The pros and cons of the method are discussed in the respective theoretical section.

1.3 Objectives and overview of the thesis

The objectives of the dissertation are focused on the development of a specific tool for the investigation of possible existing wind blade geometry adjustments that can benefit its optimal outputs in particular operational conditions described by aerodynamic, economic, environment emissions and local wind parameters. The possibilities to use different commercially and non-commercially used theories for the analysis and search procedures shall be investigated and sufficient arguments derived for the usage of proposed theories. The tool is then used for the test optimization of a particular wind turbine blade. The sensitivity analysis shall show the dependence of the outputs on the

provided inputs, as well as its relative and absolute divergences and instabilities. The pros and cons of the proposed technique shall be seen from the practical implementation, which are then documented in the results, analysis and conclusion sections.

Based on the literature review, the objectives of this thesis are the following:

- to determine the aerodynamic, mechanic, economic and noise emission parameters characterizing the wind turbine blade geometry production and operation and to summarize the analysis background for the calculation of these characteristics,
- to develop an optimization technique for the blade geometry design procedure based on the newly introduced multiobjective approach with the desirability function objective and differential evolution algorithm search method,
- to create an easy-to-apply tool, software package, for the wind blade geometry design and optimization and
- to check the methodology robustness on a practical example of a big scale wind turbine blade.

The theory background for the analysis and optimization tools are mainly driven from public sources and developed by side authors, requiring, however, assembling into one construction and disclosure of core assumptions and clarification for several parameters. The author claims the originality of the desirability function implementation for wind blade geometry optimization as a decision making tool. The investigation of various differential evolution strategies' capabilities implemented particularly for the analysis and characteristics minimization and maximization problems are carried solely by the author within the thesis. The methodology allows driving new blade design trade-offs, which might point out minor blade geometry adjustments and lead to its better performance under particular operation conditions.

The input information provided by the designer is processed with respective analysis and optimization tools. The general structure of the program with the analysis and optimization blocks is presented in Figure 1.1.

The first step is the analysis of the initial blade geometry from the aerodynamic, economic, mechanic and noise perspectives. Then the differential evolution algorithm is applied for the search of optimum values (minimum or maximum) of the respective objective functions. The desirability function approach indicates the compromise multiobjective solution.

The work is divided into five sections. Excluding the Introduction seen above, it evolves from the theory background into practical examples and conclusions.

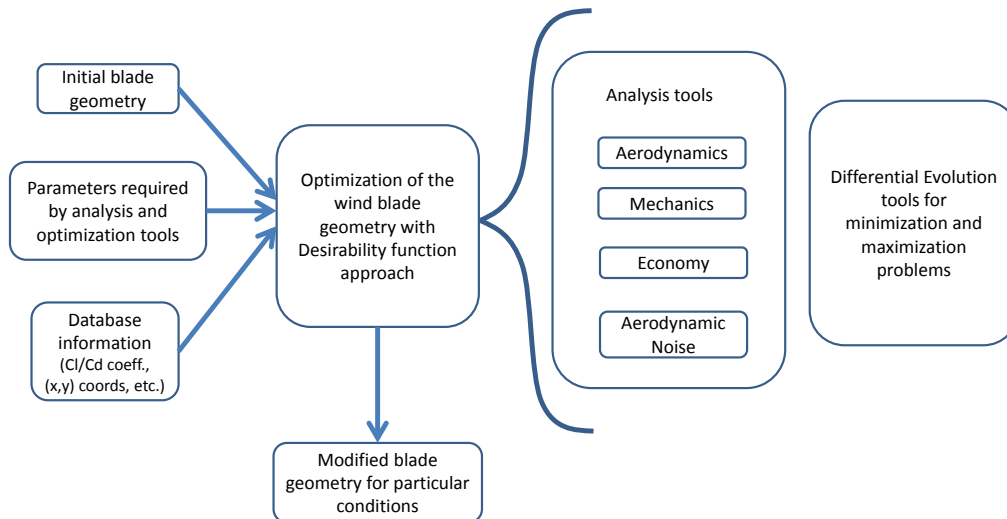


Figure 1.1: General structure of blocks for the blade geometry optimization program

Chapter 2 introduces the analysis tools for the calculation of aerodynamic, mechanic, economy and noise parameters affected by the blade geometry in conjunction with the production and operation conditions, both economic and wind.

Chapter 3 gives the theory background for the optimization tools, desirability function approach and differential evolution algorithm. The novelty of its particular implementation for multiobjective wind blade geometry optimization is shown and discussed.

Chapter 4 reveals the results of the practical optimization process investigation with respect to the WindPACT 1.5 MW turbine of the National Renewable Energy Laboratory (NREL). Sensitivity analysis of the output measures to the input parameters vector is discussed with comprehensive arguments.

Chapter 5 concludes the thesis with an overview of the work, the chosen objectives, methods of analysis and optimization, and signifies the achieved results. The possible prospects for future tasks are presented in the end of the chapter.

The Appendixes include the description of software package which has been developed by the author during the work to enhance and automate the blade geometry optimization. The software simplifies the optimization tool for a novice user. The Matlab program code listing given afterwards can be used for the further development of the analysis and optimization tools.

2 Analysis blocks

2.1 Aerodynamics

In the blade geometry optimization procedure, a large number of possible variants has to be considered. Although the capacities of modern industrial computers are growing fast, they are still not capable of solving big scale problems with methods involving Computational Fluid Dynamics (CFD). The engineering approaches are still prevailing. The industrial standard for aerodynamic calculations is the Blade Element Momentum Method (BEMM or shortly BEM). It is a linear iterative approach for the estimation of auxiliary aerodynamic parameters like the angle of the flow attack (incidence) and axial and tangential induction factors—and most importantly and interestingly—the aerodynamic blade efficiency. The unknowns are calculated on the basis of the provided blade geometry and operational conditions.

The essence of the Blade Element Method is to divide the turbine blade into a finite number of cross-sections. The finite blade length between the two nearest cross-sections is called the blade element. The relative angles of attack and consequently the induction factors and incidences are found for each blade cross-section and averaged for the elements. The found measures allow the calculation of the aerodynamic efficiency, lift and drag forces and coefficients.

For the steady-state attached flow conditions below the stall effect, BEM performs reasonably well and predicts the flow behaviour parameters with sufficient accuracy (Tangler and Bir, 2004). However, in stalled conditions, the BEM over predicts the blade efficiency due to the simplifications of the method. Among them are the uniform inflow around the blade element, which in fact is not uniformly distributed, and the assumption of no interaction between blade elements, which neglects the strong effect of trailing vorticity on the load distribution and consequent flow angle (Tangler, 2002).

The rotational torque of turbine rotor is created with the extraction of incoming flow kinetic energy. The free incoming flow with the wind velocity V_1 in Figure 2.1 passes the turbine rotor, transfers its kinetic energy to the rotor while changing its speed from V_2 to V_3 and obtains the wind speed V_4 at the long distance from the rotor.

Induction factors a and a' in Equation 2.1 are the relative measures of the axial and tangential flow wind speed reduction which passes through the turbine rotor:

$$\begin{aligned} a &= \frac{V_1 - V_2}{V_1} \\ a' &= \frac{\omega}{2\Omega} \end{aligned} \tag{2.1}$$

radius is called the tip speed ratio, and its local value, depending on the element radial distance r , is calculated as:

$$\lambda_r = \frac{\omega r}{V_1} \quad (2.3)$$

Substituting Equation 2.3 in Equation 2.2, the relative angle of attack receives a new form as Equation 2.4:

$$\beta = \arctan\left(\frac{\lambda_r(1+a')}{(1-a)}\right) \quad (2.4)$$

From Figure 2.2 and the following remark about the collective angle, the flow angle of attack (incidence angle) is found as:

$$\alpha = \beta - \gamma - p \quad (2.5)$$

The lift and drag forces acting on the blade element are determined as:

$$L = \frac{1}{2} \rho V_{rel}^2 c C_l \quad (2.6)$$

$$D = \frac{1}{2} \rho V_{rel}^2 c C_d \quad (2.7)$$

where ρ is the air density, assumed constant and equal to 1.225 kg/m^3 , and C_l and C_d are the lift and drag coefficients for a particular cross-section airfoil, angle of attack and Reynolds number. The values are given either experimentally or with modelling. There are many literature sources with presented characteristics (Bertagnolio et al., 2001; Bertagnolio et al., 2006; NREL airfoil catalogue, 2013; Somers, 2005), which are used to form the airfoil database. Section 2.1.1 reveals detailed information about the collected data and the way of storage.

The Momentum and Blade Element Theories derive the following two equations for induction factors:

$$\begin{aligned} \frac{a}{1-a} &= \frac{\sigma(C_l \cos \beta + C_d \sin \beta)}{4Q \sin^2 \beta} \\ \frac{a'}{1-a} &= \frac{\sigma(C_l \sin \beta - C_d \cos \beta)}{4Q \lambda_r \cos^2 \beta} \end{aligned} \quad (2.8)$$

where

$$Q = Q_1 Q_2 = \frac{2}{\pi} \arccos \left(e^{-\frac{3(R-r)}{2r \sin \beta}} \right) \cdot \frac{2}{\pi} \arccos \left(e^{-\frac{3(r-R_{hub})}{2R_{hub} \sin \beta}} \right) \quad (2.9)$$

is the multiplication of Prandtl corrections accounting for tip and hub vortex losses and leading to the reduction of axial and tangential forces acting on the blade.

Parameter σ is the local element solidity and equates to:

$$\sigma = \frac{Bc}{2\pi r} \quad (2.10)$$

where B stands for the number of blades, which is 3 for a classical HAWT

- c – the local cross-section chord
- r – the radial distance of the cross-section from the hub centre

The connection of the induction factors to the lift and drag coefficients as well as the relative angles of attack shown in Equation 2.8 lead to the iterative nature of the solution search.

The calculation of the axial and tangential induction factors with respective angles of attack, lift and drag characteristics for each blade element starts from the initial guess with unit loss corrections and zero drag coefficient:

$$\beta = \frac{2}{3} \arctan \left(\frac{1}{\lambda_r} \right) \quad (2.11)$$

Lift and drag coefficients are determined with the airfoil type and incidence angle based on Equation 2.5. The tip and hub loss factors are obtained with Equation 2.9. The unknown parameters in Equation 2.8 are available to calculate a guess of a and a' values.

The BEM theory falls down when the axial induction factor is greater than 0.5. According to BEM, the flow shall reverse in the far wake, which is not happening. The real phenomenon in the far wake is the increase of the flow turbulence level. To account for that, Glauert (1926) came up with a correction to BEM which brings its results in accordance with the experiments (see Figure 6 and Figure 7 in (Moriarty and Hansen, 2005)). This is called the classical BEM now.

The correction math is presented as follows in the case of $a > 0.5$. Otherwise the simple BEM equations are applied (Hansen, 2008):

$$a = \frac{1}{2} \left(2 + 0.2K - \sqrt{(2 + 0.2K)^2 + 4(0.16K - 1)} \right) \quad (2.12)$$

where

$$K = \frac{4Q \sin^2 \beta}{\sigma (C_l \cos \beta + C_d \sin \beta)} \quad (2.13)$$

After the first guess initialization the described steps are continued iteratively until the induction factors reach stable values with respective tolerances ε_a and $\varepsilon_{a'}$. For the rest of the iterations, except for the initialization step, the relative angle of attack is calculated with Equation 2.4.

$$\begin{aligned} \varepsilon_a &= 1 - \frac{a_i}{a_{i+1}} \\ \varepsilon_{a'} &= 1 - \frac{a'_i}{a'_{i+1}} \end{aligned} \quad (2.14)$$

2.1.1 Lift and drag characteristics

The main experimental or modelling parameters of the airfoils are lift and drag characteristics, i.e. lift and drag dependence on the Reynolds number and angle of attack. The curves are typically presented in graphical or tabular form.

The lift and drag curves of different airfoils behave in a similar way. Therefore, by describing the particular important points of the dependencies we can reduce the volume of the data to be stored. The method of short lift and drag curve presentation and storage system has been introduced by Merz (2011).

The essence of the approach is to divide the lift and drag characteristics for piecewise functions. Figure 2.3 demonstrates the curves with the respective visual representation of the flow behaviour on various lift and drag regions.

The characteristic points marked with coordinates (α_i, C_i) on the curves are the ones to be stored in the designer database and to be used later to rebuild lift and drag coefficient values for the intermediate angles of attack. The four regions (A)–(D) are represented with different functions as follows.

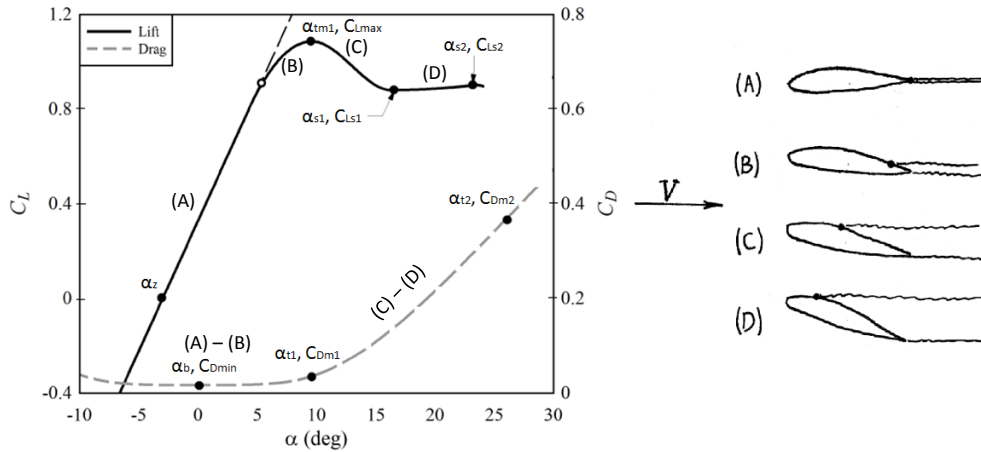


Figure 2.3: Lift and drag curves with the describing parameters represented, based on Merz (2011)

(A): The flow is fully attached. Linear behaviour of the lift curve and polynomial behaviour of the drag curve.

The lift coefficient is described with the following equation:

$$C_l = \gamma_a (\alpha - \alpha_z) \quad (2.15)$$

where $\gamma_a = 0.11$ – is the assumed slope of the lift curve (1/deg)

α – intermediate angle of attack

α_z – the angle of attack corresponding to zero lift coefficient

The drag function is described with fourth order polynomial intersecting points ($\alpha_b, C_{Dmin}=0$) and (α_{t1}, C_{Dm1}):

$$C_d = K (\alpha - \alpha_b)^4 + C_{dmin} \quad (2.16)$$

where

$$K = \frac{C_{dm1} - C_{dmin}}{(\alpha_{t1} - \alpha_b)^4} \quad (2.17)$$

(B): The flow starts to separate from the trailing edge. A circle segment type of behaviour for the lift.

This region is described for the lift curve as a circle segment equation.

$$C_l = C_{l_{\max}} - R_c + \sqrt{R_c^2 - (\alpha - \alpha_{m1})^2} \quad (2.18)$$

where R_c is the radius of the circle

$$R_c = \frac{\gamma_a(\alpha_{m1} - \alpha_z) - C_{l_{\max}}}{\sin(t_i) - \gamma_a \cos(t_i) - 1} \quad (2.19)$$

and t_i is the segment angle in radians

$$t_i = \arctan(\gamma_a) + \frac{\pi}{2} \quad (2.20)$$

The drag coefficient in this region is calculated the same way as for region (A)

(C): The extensive separation of the flow which proceeds toward the leading edge. Polynomial equation for the lift and linear for the drag.

The third order polynomial is used to describe the lift curve behaviour:

$$C_l = C(1)\alpha^3 + C(2)\alpha^2 + C(3)\alpha + C(4) \quad (2.21)$$

where $C=A\backslash B$ is the matrix of polynomial coefficients:

$$A = \begin{bmatrix} \alpha_{m1}^3 & \alpha_{m1}^2 & \alpha_{m1} & 1 \\ 3\alpha_{m1}^2 & 2\alpha_{m1} & 1 & 0 \\ \alpha_{s1}^3 & \alpha_{s1}^2 & \alpha_{s1} & 1 \\ 3\alpha_{s1}^2 & 2\alpha_{s1} & 1 & 0 \end{bmatrix} \quad (2.22)$$

$$B = \begin{bmatrix} C_{l_{\max}} \\ 0 \\ C_{ls1} \\ \frac{C_{ls2} - C_{ls1}}{\alpha_{s2} - \alpha_{m1}} \end{bmatrix}$$

The drag coefficient has the linear expression on this and further regions:

$$C_d = (C_{dm2} - C_{dm1}) \frac{\alpha - \alpha_{t1}}{\alpha_{t2} - \alpha_{t1}} + C_{dm1} \quad (2.23)$$

(D): The flow remains separating, although the separation point is fixed and the flow is attached close to the leading edge. The expressions for both lift and drag curves are linear on that region.

$$C_l = (C_{ls2} - C_{ls1}) \frac{\alpha - \alpha_{s1}}{\alpha_{s2} - \alpha_{s1}} + C_{ls1} \quad (2.24)$$

The lift and drag curve spectrum is described for incidences around 40–45 degrees. In practice the incidences are not exceeding that limit for pitch regulated wind turbines. The lift curve is mirrored about the X axis for angles of attack smaller than α_z , and the drag curve is mirrored about the Y axis for intermediate incidences smaller than α_b . The assumption is valid for the whole range of airfoils' lift and drag characteristic found by the author.

The advantage of the proposed approach over look-up table is its predetermined volume of data needed to be stored, as well as known functional dependency. On the contrary, the look-up table requires higher density of the data representation in the stall and bending regions on the lift curve to derive accurate result.

In the present thesis, the lift and drag curves are assumed to be independent of Reynolds number, as for the case of variable speed pitch regulated wind turbine, the Reynolds number variation is minor and less are the lift and drag characteristics changes. The independent study for the original WindPACT 1.5 MW variable speed pitch regulated turbine blade (see the blade description in section 4.1) showed that the Reynolds number variation range is $[2.4; 3.7] \cdot 10^6$ in which the change of airfoils lift and drag properties in the pre-stall region is negligibly small.

Consequently, the design of the optimum blade geometry is carried out for the design wind speed, and it spreads for the whole range of normal (not extreme) operating conditions. In addition, the aerodynamic procedure is carried out for the extreme wind speed for further mechanics investigation based on the induced normal and inplane forces under these conditions. According to IEC standard (IEC 61400-12-1, 2005), the 50-year 10-minute extreme wind speed is five times greater than the annual mean wind speed.

2.1.2 Aerodynamic power coefficient, forces and moments

The flow measures along the blade and its elements (angles of attack, induction factors, local tip speed ratio, etc.) found by the procedure of section 2.1 are used for the calculation of the main aerodynamic outputs: the power coefficient, axial and tangential forces and moments acting on the blade elements from the flow side.

The aerodynamic power coefficient is defined as the ratio of the aerodynamic power P produced by the wind turbine to the overall power of the incoming flow, P_{wind} . Ingram

(2011) derives the power coefficient from the values of induction factors, relative angles of attack, tip and hub losses:

$$C_p = \frac{P}{P_{wind}} = \frac{8}{\lambda^2} \int_{\lambda_r}^{\lambda} Q \lambda_r^3 a'(1-a) \left[1 - \frac{C_d}{C_l} \tan \beta \right] d\lambda_r \quad (2.25)$$

The calculation can be implemented with the trapezoid rule:

$$\int_{x_o}^{x_n} f(x) dx \approx \frac{x_n - x_o}{2n} [(y_o + y_n) + 2(y_1 + y_2 + \dots + y_{n-1})] \quad (2.26)$$

Here $n=1$ is the respective degree of accuracy, x is replaced with λ_r and the function f is $f(x) = Q \lambda_r^3 a'(1-a) [1 - C_d / C_l \tan \beta]$. The rule is applied to each blade element, and while summarized, gives the value of the integral aerodynamic power efficiency coefficient.

The forces and moments, both normal to the rotational plane and inplane, induced by the incoming wind flow affect the blade structure buckling, its deflection and rotation. The further economic and mechanic property investigations of the blade geometry described in section 2.2 are primarily influenced by the forces and moments acting on the blade surface, i.e. its elements.

The normal and in plane (tangential) forces for each blade element are found with the lift and drag forces and their relative angles of attack:

$$p_n = L \cos \beta + D \sin \beta \quad (2.27)$$

$$p_t = L \sin \beta - D \cos \beta \quad (2.28)$$

The linear distribution of forces along the element between the two cross-sections of the blade implies a linear equation:

$$p_t = A_i r + B_i \quad (2.29)$$

where $A_i = \frac{p_{t,i+1} - p_{t,i}}{r_{i+1} - r_i}$, $B_i = \frac{p_{t,i} r_{i+1} - p_{t,i+1} r_i}{r_{i+1} - r_i}$

The torque of the finite blade element length dr is then

$$dM = r p_t dr = (A_i r^2 + B_i r) dr \quad (2.30)$$

Finally, the overall torque is the sum of elemental torques multiplied with the number of blades, $B=3$:

$$M_{tot} = B \sum_{i=1}^{N-1} \frac{1}{3} A_i (r_{i+1}^3 - r_i^3) + \frac{1}{2} B_i (r_{i+1}^2 - r_i^2) \quad (2.31)$$

2.2 Mechanics

According to Hansen (2008), the three most significant forces acting on the wind blade are the gravitational, inertial and aerodynamic loadings.

The present study eliminates the gravitational and inertial forces because the first one is a cyclic load which on average is compensated during the rotor revolution and the second one is negligible with a small acceleration rate while the turbine rotates within the studied stable conditions. The aerodynamic force is the source of blades rotation, torque, but deflections as well. The normal and inplane forces contribute to flapwise and edgewise deflections, respectively.

The fatigue loads play the major role while designing the final geometry of the wind turbine blade, and it may dominate over extreme load concerns (Bir, 2001). However, the fatigue loads are dependent on the overall wind turbine structural behaviour and unknown on the preliminary design stages. The measurements or the modellings of the fatigue loads require special expertise, complicate the analysis tool and rapidly increase the optimization search time. The large safety factors applied to static loads and moments under extreme wind conditions account for modelling assumptions and uncertainties while designing preliminary wind blade geometry.

The above-mentioned is partly also a justification for the use of the chosen iterative design approach instead of the Finite Element Method (FEM). Moreover, the method consumes large CPU times and is likely more an analysis tool than a design one, as it shall be used repeatedly while the designer modifies the laminate organisation and runs the analysis until the structure meets the mechanical criteria.

The wind blade mechanic investigation is based on the calculation of proper blade material thicknesses to withstand the induced aerodynamic loads. The blade is divided into elements, and with the calculated structural characteristics of its cross-sections based on material physical properties and their thicknesses, the beam theory (Hansen, 2008) can be applied to compute the stresses and deflections of the blade. It is used afterwards iteratively for the search of sufficient material thicknesses for each blade element to fulfil simultaneously three criteria and to compose the preliminary wind blade geometry:

- The blade tip deflection shall not exceed 1/3 of the static blade-tower clearance, L (Tong, 2010).
- The blade structure shall withstand the ultimate strength.
- The blade structure shall withstand the buckling.

The blade tip normal and inplane deflections, $defl_z$ and $defl_y$, are summarized with the Pythagorean theorem to derive the final deflection. The process of deflections calculation is expressed in the beam theory sequence of equations described later in section 2.2.2.

The ultimate strength inequality expresses the rule that the axial stress at any point of the blade cross-section with span distance z shall not exceed the allowable stress σ_z for these points in 50-year 10-minute extreme wind conditions:

$$M_z^{ext} E(x, y) \frac{[EI_{y'}](y - y_e) - [ED_{x'y'}](x - x_e)}{[EI_{x'}][EI_{y'}] - [ED_{x'y'}]^2} \leq \sigma_z^a(x, y) \quad (2.32)$$

The allowable stress σ_z^a is the multiplication of the ultimate strength σ_z^u , compressive or tensile, with the safety factor SF . The ultimate strength is found based on the structural properties of the blade cross-section, as well as the moments of stiffness inertia EI and moment of centrifugal stiffness ED .

The buckling criterion equation implies that the edge loading per unit peripheral length of the blade surface shall not exceed the Euler load for that surface:

$$\int \sigma_z d\tau \leq \frac{3.6\pi^2}{b^2} \int \frac{E\tau^2}{1-\nu^2} d\tau \quad (2.33)$$

The axial compressive stresses are integrated over the surface thickness on the left side of Equation 2.33. The parameter τ is the distance of the panel material point (x, y) from the neutral surface, shifted on $x_{na}=0.314$ from the airfoil leading edge. Effective Young's modulus E is pre-calculated with the structural properties of the cross-section.

The procedure of structural property calculation is described in section 2.2.1. The essence of the blade beam theory for the investigation of stresses and deflections is described later in section 2.2.2.

2.2.1 Structural properties of the blade cross-section

The wind turbine blade cross-section consists of material plies which form the shape of the cross-section airfoil and structural web or webs which provide the construction rigidity. The typical blade section structure is presented in Figure 2.4.

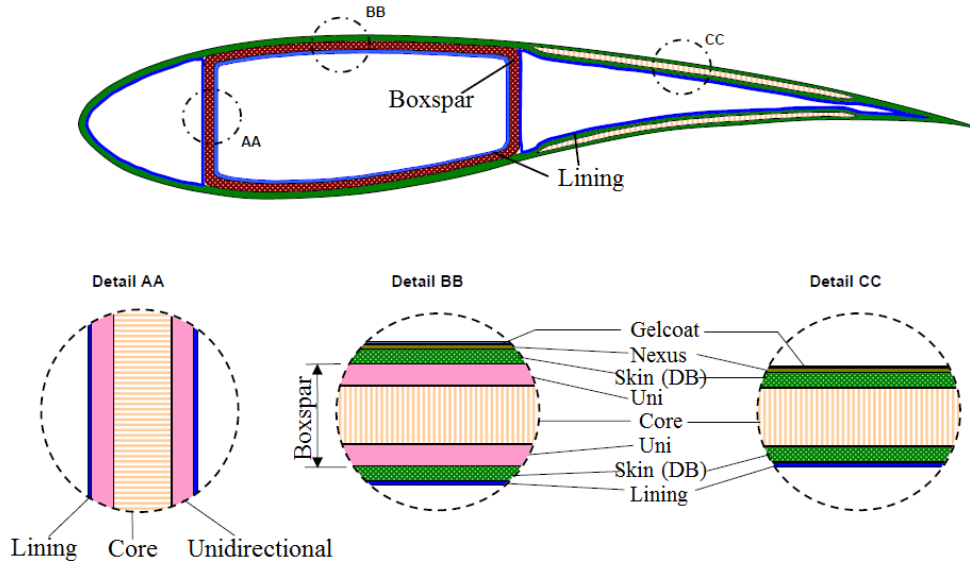


Figure 2.4: Structural configuration of blade cross-section (Bir and Migliore, 2004)

The construction in Figure 2.4 has the box spar configuration of the structural webs. Another possible and applied inner construction is a D-spar configuration with only one structural web from the suction and pressure sides of the airfoil.

The mechanical properties of each ply layer used in the blade manufacturing are summarized in Table 2.1.

Table 2.1: Mechanic and geometric data for used structural materials (Bir and Migliore, 2004)

Material	t_{ply} (mm)	E (Pa)	σ_{ut} (Pa)	σ_{uc} (Pa)
Gelcoat	0.381	--	--	--
Nexus	0.51	--	--	--
Double-bias	0.53	1.03E+10	1.51E+8	-1.74E+8
Lining	0.53	1.03E+10	1.51E+8	-1.74E+8
Unidirectional	0.53	3.70E+10	9.86E+8	-7.46E+8
Core	3.125	1.00E+07	--	--

The public sources of the airfoils coordinates (Airfoil coordinates catalogue, 2013; Profili software, 2013; Drela and Youngren, 2001) contain (x,y) points of the airfoil surface from the leading toward trailing edges. According to Bir and Migliore (2004), the box spar structural webs are positioned on 12% and 50% of the chord. The positioning is done on the preprocessing stage of the airfoil characteristic data collection and its storage in the database.

The structural layers containing various materials presented in Figure 2.4 with their respective properties in Table 2.1 are defined by the minimum layer thickness t_{ply} multiplied with the integer number of plies m_{ply} .

Mechanical procedure calculations require a single result output, which is the blade structural thickness. The equation introduced in the present thesis summarizes the found layer thicknesses while averaging the core thicknesses of the middle and trailing edge sections:

$$t_{all} = t_{uni} + t_{db} + \frac{1}{2}(t_{core}^{te} + t_{core}^{mid}) + t_{li} \quad (2.34)$$

The structural parameters of the blade cross-section determining its mechanical behaviour are presented in Figure 2.5 for the box spar configuration of the inner webs considered for the present thesis.

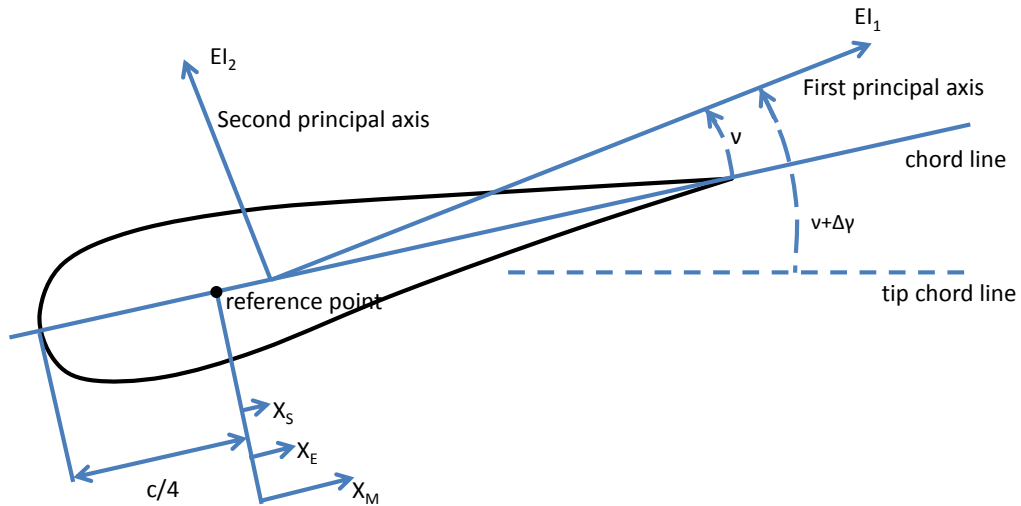


Figure 2.5: Structural parameters of the blade cross-section (Hansen, 2008)

The definition of structural parameters starts from the calculation of the effective Young's modulus $E(x,y)$ and the effective allowable axial compressive stress $\sigma(x,y)$ for the points of cross-section details AA, BB and CC shown in Figure 2.4. The mixture rule, explained in the basic theoretical books for structural mechanics (Yadama, 2007), is applied for deriving the effective values from its components.

The Young's modulus E_{AAy} and the axial compressive stress σ_{AA} in Figure 2.4 (AA) are calculated with Equations 2.35 and 2.36, respectively

$$E_{AAy} = \frac{2(t_{li} + t_{uni}) + t_{core}}{2\left(\frac{t_{li}}{E_{li}} + \frac{t_{uni}}{E_{uni}}\right) + \frac{t_{core}}{E_{core}}} \quad (2.35)$$

$$\sigma_{AA} = \frac{\sigma_{lin} + \sigma_{uni}}{E_{lin} + E_{uni}} E_{AAy} \quad (2.36)$$

All points of the detail AA are assumed to be compressed, and the core stress properties are not included as unknown for the particular case.

Detail BB:

$$E_{BBy} = \frac{2(E_{db}t_{db} + E_{uni}t_{uni}) + E_{li}t_{li} + E_{core}t_{core}}{2(t_{db} + t_{uni}) + t_{li} + t_{core}} \quad (2.37)$$

$$\sigma_{BBc} = \frac{2(\sigma_{db}^c + \sigma_{uni}^c) + \sigma_{lin}^c}{2(E_{db} + E_{uni}) + E_{lin}} E_{BBy} \quad (2.38)$$

The compressed value of stress is assumed for the suction (upper) side of the airfoil.

$$\sigma_{BBt} = \frac{2(\sigma_{db}^t + \sigma_{uni}^t) + \sigma_{lin}^t}{2(E_{db} + E_{uni}) + E_{lin}} E_{BBy} \quad (2.39)$$

The tensile stress is applied on the pressure (lower) side of the airfoil.

Detail CC

$$E_{CCy} = \frac{2E_{db}t_{db} + E_{li}t_{li} + E_{core}t_{core}}{2t_{db} + t_{li} + t_{core}} \quad (2.40)$$

$$\sigma_{CCc} = \frac{2\sigma_{db}^c + \sigma_{lin}^c}{2E_{db} + E_{lin}} E_{CCy} \quad (2.41)$$

$$\sigma_{CCt} = \frac{2\sigma_{db}^t + \sigma_{lin}^t}{2E_{db} + E_{lin}} E_{CCy} \quad (2.42)$$

Equations 2.41 and 2.42 are for compressed and tensiled sides of the blades, respectively.

The (X_R, Y_R) coordinates of the reference coordinate system are calculated for each element of the airfoil cross-section:

$$X_R = c \left(\frac{1}{2} (x_i + x_{i+1}) - 0.25 \right) \quad (2.43)$$

$$Y_R = c \frac{1}{2} (y_i + y_{i+1}) \quad (2.44)$$

where i stands for the element number, as the calculation procedure is done iteratively for each airfoil element, defined with collected coordinates.

The investigation proceeds with the moments of stiffness calculation in the reference coordinate system.

Longitudinal stiffness:

$$[EA] = \int_A E dA \quad (2.45)$$

Moment of stiffness about the X_R axis:

$$[ES_{X_R}] = \int_A E Y_R dA \quad (2.46)$$

Moment of stiffness about the Y_R axis:

$$[ES_{Y_R}] = \int_A E X_R dA \quad (2.47)$$

Moment of stiffness inertia about the X_R axis:

$$[EI_{X_R}] = \int_A E Y_R^2 dA \quad (2.48)$$

Moment of stiffness inertia about the Y_R axis:

$$[EI_{Y_R}] = \int_A E X_R^2 dA \quad (2.49)$$

In the presented set of equations, the elemental surface of the airfoil dA is found with element width dh and thickness δ depending on the cross-section detail (refer to Figure 2.4) into which the present element belongs to:

$$dA = \delta h = \delta c \sqrt{(x_i - x_{i+1})^2 + (y_i - y_{i+1})^2} \quad (2.50)$$

where $x_i, x_{i+1}, y_i, y_{i+1}$ are the (x, y) coordinates of the element left and right boundaries, respectively.

From the derivative Equations 2.45-2.47 the (X_E, Y_E) coordinates of the elasticity point are determined within the reference coordinate system:

$$X_E = \frac{[ES_{Y_R}]}{[EA]} \quad (2.51)$$

$$Y_E = \frac{[ES_{X_R}]}{[EA]} \quad (2.52)$$

The present study assumes that the centre of mass coincides with the elasticity point. Strictly speaking, this is possible solely in the case of the constant Young's modulus and material density all over the blade cross-sections. However, the assumption allows a significant simplification of the procedure, and according to Hansen (2008), it does not make a significant difference to the final result.

The received moment measures are transferred to the elasticity point origin with the following set of conversion equations:

$$[EI_{X'}] = \int_A EY'^2 dA = [EI_{X_R}] - Y_E^2 [EA] \quad (2.53)$$

$$[EI_{Y'}] = \int_A EX'^2 dA = [EI_{Y_R}] - X_E^2 [EA] \quad (2.54)$$

$$[ED_{X'Y'}] = \int_A EX'Y' dA = [ED_{XY_R}] - X_E Y_E [EA] \quad (2.55)$$

From here, the angle ν between the chord line and the first principal axis (see Figure 2.5) can be calculated.

$$\nu = \frac{1}{2} \arctan \left(\frac{2[ED_{X'Y'}]}{[EI_{Y'}] - [EI_{X'}]} \right) \quad (2.56)$$

The bending stiffnesses about the first and second principal axis are:

$$[EI_1] = [EI_{X'}] - [ED_{X'Y'}] \tan \alpha \quad (2.57)$$

$$[EI_2] = [EI_{y'}] + [ED_{x'y'}] \tan \alpha \quad (2.58)$$

The calculation of the structural blade parameters is used later on for the criteria of section 2.2 and within the beam theory to calculate the bending moments and mechanical deflections.

2.2.2 The static beam theory for wind turbine blade

The beam theory implies linear behaviour of the force distribution between the blade cross-sections. It summarizes the elements deflection as the linear sum of individual deflections. The blade itself is presented as a cantilever beam fixed in the root point, see Figure 2.6. The number of beams considered is equal to the given number of blade cross-sections.

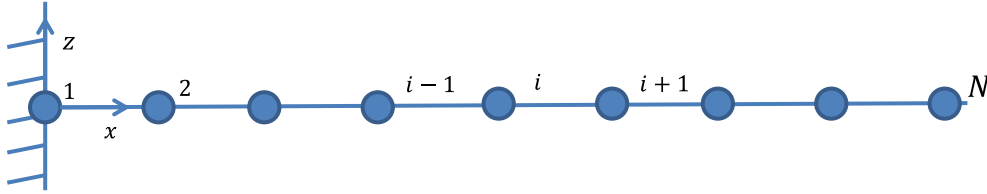


Figure 2.6: Cantilever beam representation of the wind turbine blade (Hansen, 2008)

The inplane and normal forces acting from the incoming flow on the blade surface induce shear forces and bending moments. The structural parameters calculated with the procedure of section 2.2.1 are used for the following sequence of equations to receive the tip blade deflection for the design and the extreme wind conditions. The index i represents the number of the blade cross-section starting from the blade tip toward the blade root:

The shear forces

$$T_{y,i-1} = T_{y,i} + \frac{1}{2} (p_{t,i-1} + p_{t,i}) (r_i - r_{i-1}) \quad (2.59)$$

$$T_{z,i-1} = T_{z,i} + \frac{1}{2} (p_{n,i-1} + p_{n,i}) (r_i - r_{i-1}) \quad (2.60)$$

$$T_{y,i-1}^{ext} = T_{y,i}^{ext} + \frac{1}{2} (p_{t,i-1}^{ext} + p_{t,i}^{ext}) (r_i - r_{i-1}) \quad (2.61)$$

The flapwise and edgewise bending moments

$$M_{y,i-1} = M_{y,i} - T_{z,i} (r_i - r_{i-1}) - \left(\frac{1}{6} p_{n,i-1} + \frac{1}{3} p_{n,i} \right) (r_i - r_{i-1})^2 \quad (2.62)$$

$$M_{z,i-1} = M_{z,i} - T_{y,i} (r_i - r_{i-1}) - \left(\frac{1}{6} p_{t,i-1} + \frac{1}{3} p_{t,i} \right) (r_i - r_{i-1})^2 \quad (2.63)$$

$$M_{z,i-1}^{ext} = M_{z,i}^{ext} + T_{y,i}^{ext} (r_i - r_{i-1}) + \left(\frac{1}{6} p_{t,i-1}^{ext} + \frac{1}{3} p_{t,i}^{ext} \right) (r_i - r_{i-1})^2 \quad (2.64)$$

The bending moments transformed to the principal axes, see Figure 2.5

$$M_{1,i} = M_{y,i} \cos \varphi - M_{z,i} \sin \varphi \quad (2.65)$$

$$M_{2,i} = M_{y,i} \sin \varphi + M_{z,i} \cos \varphi \quad (2.66)$$

where $\varphi = \nu + \Delta\gamma = \nu + (\gamma_{end} - \gamma_i)$ is the angle between the first principal axis and the tip chord line.

The curvatures about the principal axes transformed to the flapwise and edgewise axes of the blade

$$k_{z,i} = - \frac{M_{1,i}}{[EI_{1,i}]} \sin \varphi + \frac{M_{2,i}}{[EI_{1,i2}]} \cos \varphi \quad (2.67)$$

$$k_{y,i} = \frac{M_{1,i}}{[EI_{1,i}]} \cos \varphi + \frac{M_{2,i}}{[EI_{1,i2}]} \sin \varphi \quad (2.68)$$

The deflection calculation starts from the blade root and continues towards the blade tip for each blade element with the boundary conditions of zero angular θ and linear u deflections at the blade root: $\theta_{y,1} = 0$; $\theta_{z,1} = 0$; $u_{y,1} = 0$; $u_{z,1} = 0$.

The angular deformation

$$\theta_{y,i+1} = \theta_{y,i} + \frac{1}{2} (k_{y,i+1} + k_{y,i}) (r_{i+1} - r_i) \quad (2.69)$$

$$\theta_{z,i+1} = \theta_{z,i} + \frac{1}{2} (k_{z,i+1} + k_{z,i}) (r_{i+1} - r_i) \quad (2.70)$$

The linear deflection

$$u_{y,i+1} = u_{y,i} + \theta_{z,i} (r_{i+1} - r_i) + \left(\frac{1}{6} k_{z,i+1} + \frac{1}{3} k_{z,i} \right) (r_{i+1} - r_i)^2 \quad (2.71)$$

$$u_{z,i+1} = u_{z,i} - \theta_{y,i} (r_{i+1} - r_i) + \left(\frac{1}{6} k_{y,i+1} + \frac{1}{3} k_{y,i} \right) (r_{i+1} - r_i)^2 \quad (2.72)$$

The tip deflection is derived for the last investigated cross-section with the Pythagorean theorem and values u_z , u_y :

$$\Delta_{defl}^{tip} = \sqrt{u_{y,end}^2 + u_{z,end}^2} \quad (2.73)$$

Finally, it is possible to calculate the stresses σ for every point of the blade cross-sections:

$$\sigma_z(x, y) = E(x, y) \varepsilon(x, y) \quad (2.74)$$

where ε is the structure strain:

$$\varepsilon(x, y) = \frac{M_1}{[EI_1]} y - \frac{M_2}{[EI_2]} x \quad (2.75)$$

2.3 Economics

The importance of the wind turbine economic performance and its investigation is marked in a great number of studies (Xudong et al., 2009; Zaaier, 2003). The research is concentrated on delivering a robust methodology and development of common economic parameters which could express the turbine operation from a sufficient number of perspectives.

Among the common economic measures is the Levelized Cost of Energy, presented by Zaaier (2003). The quite extensive economic estimation takes into account the economic evaluations of the major wind turbine components like blade, generator, nacelle, tower, foundation and grid connection.

Another economic theory has been presented by Xudong et al. (2009). This work speculates particularly the wind turbine blade cost model instead of a full turbine set of components.

The blade cost is divided into fixed and variable components. Xudong classifies the transportation, installation and operation expenses among the components of wind blade fixed costs. These are relatively small compared to the blade production costs, which

are mainly comprised of variable material expenses, design procedure costs and direct labour expenses. The latter are related to the variable component of the overall blade cost.

The economic function, the relative rotor cost C_{rotor} is:

$$C_{rotor} = b_{rotor} + (1 - b_{rotor})w_{rotor} \quad (2.76)$$

where

b_{rotor} – the fixed rotor cost component

w_{rotor} – the variable rotor cost component

For the present study, the fixed component $b_{rotor}=0.1$ is based on the work of Xudong et al. (2009).

The variable rotor cost component is derived with the relative material usage and attributed to the relative difference in mass multiplied by the elemental chord between the initial blade geometry and intermediate shape considered within the optimization procedure:

$$w_{rotor} = \sum_{i=1}^N \frac{m_i c_i}{M_{tot} c_{i,or}} \quad (2.77)$$

where

m_i – the mass of the i -th blade element

c_i – the average chord of the i -th blade element

M_{tot} – the total mass of the original blade geometry

$c_{i,or}$ – the average chord of the i -th element of the original blade geometry

N – the total number of blade elements

The average chord of the blade element is the mean value of two chords: the ‘root’ and ‘tip’ sides of the element. The elemental and consequently the blade mass are found with the following assumptions:

- Due to the close values of material densities used in the wind turbine blade design and considered for mechanical investigation, the material density difference has been neglected and assumed to be constant for the entire blade.
- The material cost model takes the outer blade geometry solely into account and does not include the internal webs and hub connecting rods.

The assumptions allow deriving the transformed equation for the relative material usage:

$$w_{rotor} = \sum_{i=1}^{i=N} \frac{S_i \delta_i c_i}{S_{orig} \delta_{orig} c_{orig}} \quad (2.78)$$

where the values of the element surface area, S , and the material thickness δ are denoted in Figure 2.7.

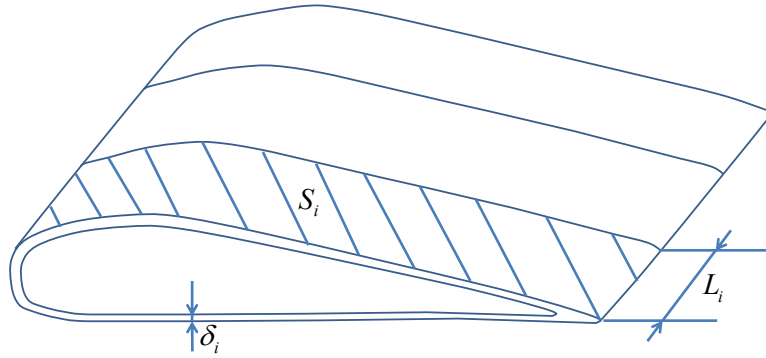


Figure 2.7: Geometry parameters of blade element

The element surface area is approximately determined with the average cross-section perimeter and the element length L_i , taking into account the element twist $\Delta\gamma$ and the blade span distance dr :

$$S_i = P_i L_i \quad (2.79)$$

$$L_i = dr_i / \cos \Delta\gamma_i \quad (2.80)$$

where P_i is the average cross-section perimeter calculated with the unit airfoil perimeter and element chord

$$P_i = \frac{1}{2} (c_b P_b^1 + c_e P_e^1) \quad (2.81)$$

The subscript b is related to the root (begin) side of the element, the subscript e to the tip (end) side of the element and superscript 1 to the unit measure. The airfoil unit perimeter is contained in the database with the rest of the relevant information: lift and drag coefficients and airfoil (x,y) unit coordinates.

2.4 Aerodynamic noise model

Aerodynamic noise models are constantly developed (Brooks et al., 1989; Fuglsang and Madsen, 1996; Lowson, 1993; Tadamas and Zangeneh, 2011) to respond to the concerns about the visual and pollution (both noise and waste) effects of human

activities. The existing models are usually based on CFD simulations or on semi-empirical calculations, which require calibration and corrections for a particular implementation case.

The noise emission modelling is an important part of the wind turbine design process. The recognized standards for noise emission limits (AWEA standard 2.1, 1989; IEC 61400-11, 2001) determine the turbine placement in the terrain as well as the turbine design itself. For example, due to the aerodynamic noise constrains the linear tip rotational speed of onshore turbines is limited to approximately 65 m/s (Rogers and Manwell, 2002), while the same parameter for offshore turbine may reach higher values as the noise and visual impacts in offshore conditions are not as crucial as in onshore cases.

In addition to aerodynamic noise, there are mechanical and electrical noises as well. Mechanical noise can be suppressed with traditional methods, for example grease, and electrical noise is the task of a separate study, although they are both usually neglected due to their low levels compared to aerodynamic noise. The present thesis investigates the aerodynamic noise emissions solely.

The origin of the noise modelling is based on the Lighthill acoustic analogy and the solution of Navier-Stokes equations (Lowson, 1993). Fuglsang and Madsen (1996) used a semi-empirical solution based on the model of Brooks et al. (1989) providing a much faster approach.

Brooks et al. (1989) conducted a sophisticated validation study of their noise emission model against three independent measurements carried out at the United Technologies Research Center (UTRC) by Schlinker and Amiet (1981), Schlinker (1977) and Fink et al. (1976). The experimental validation concluded on the successful application of the noise emission model for helicopter rotor and expressed confidence on its applicability for wind turbine blades self-induced aerodynamic noise. Although the work has been validated on NACA 0012 profile, it is used for practical calculations of other types of profiles, due to the lack of sufficient experimental data.

According to Fuglsang and Madsen, the overall aerodynamic noise is composed of three main components, which are divided into subcomponents themselves. Each component can be modelled individually, and the overall noise emission is summarized with the interference law. Following Lowson (1993), the list of the main noise components is:

- Discrete frequency noise at the blade passing frequency and its harmonics
- Self-induced noise
 - Trailing Edge noise
 - Separation-stall noise
 - Tip Vortex Formation noise
 - Laminar Boundary Layer Vortex Shedding noise

- Trailing Edge Bluntness Vortex Shedding noise
- Turbulent Inflow noise

According to Lowson's investigation, the self-induced noise is dominant at low wind speeds and low rotations of the blade while the noise due to the turbulent inflow is dominant at high wind speeds. In his analysis, the importance of the noise sources for the overall result proved that the noise emissions model can be sufficiently accurate while the two main sources are considered: the trailing edge and turbulent inflow noises. Therefore, the present thesis eliminates the modelling of the rest noise components.

When these two components are derived, the interference law is applied to get their summarized value:

$$L_p^{total} = 10 \log \left(10^{0.1L_p^{TE}} + 10^{0.1L_p^{TI}} \right) \quad (2.82)$$

The following subsections describe the calculation of the two main aerodynamic noise components.

2.4.1 Turbulent inflow noise

Every free flow contains turbulence. Turbulence creates an unequal pressure distribution on the blade surface and leads to aerodynamic noise emissions. The wind turbine noise can be decomposed to a range of frequencies and emitted at all of them, affecting the overall background noise of terrain.

Due to the turbulence noise decomposition into a range of frequencies, the overall turbulence noise value, L_{pn}^{TI} , can be considered as a root mean square of its frequency components, L_{pf}^{TI} :

$$L_{pn}^{TI} = \sqrt{\sum_F (L_{pf}^{TI})^2} \quad (2.83)$$

where F stands for the range of considered frequencies. The range of octave band frequencies corresponding to aerodynamic noise investigation is: $F = \{63, 125, 250, 500, 1000, 2000, 4000, 8000\}$ Hz. These are called A -band frequencies. The unit of sound pressure level is therefore indicated as dB(A). The noise level calculated for each frequency of the range F is determined with the following equation:

$$L_{pf}^{TI} = 58.4 + 10 \log \left[\rho^2 c_0^2 l \frac{L}{r^2} M^3 I^2 k^3 (1+k^2)^{-7/3} \right] + 10 \log \left(\frac{LFC}{1+LFC} \right) \quad (2.84)$$

where

L – the length of the free stream turbulent flow

I – the turbulence intensity

k – the blade cross-section wave number, $k = \pi f c_{av} / V_{rel}$

c_{av} – is the average chord of the blade element

V_{rel} – the blade element relative wind speed found from the aerodynamic procedure, see section 2.1

c_0 – the sound of speed in the air for standard ambient conditions assumed constant in all investigations, 340 m/s

LFC – is the low frequency correction factor:

$$LFC = 10S^2 M k^2 / q^2 \quad (2.85)$$

where S^2 – the squared compressible Sears function:

$$S^2 = \left(\frac{2\pi k}{q^2} + \frac{1}{1 + 2.4k / q^2} \right)^{-1} \quad (2.86)$$

where $q^2 = 1 - M^2$ – the coefficient related to Mach number $M = V_{rel} / c_0$.

The sound pressure level calculated by Equation 2.83 for the frequency range F and each blade element is summarized with the interference law:

$$L_p^{TI} = 10 \log \left(\sum_{i=1}^N 10^{0.1 L_{pm}^{TI}} \right) \quad (2.87)$$

where N is the total number of blade elements, which is equal to the number of blade cross-sections minus one.

The length of the turbulent flow, L , and the value of the turbulence intensity, I , used for Equation 2.84 are attributed to the considered free stream wind speed class, defined with the initial information of the designer. According to the IEC standard (IEC 61400-1, 2005), there are four wind speed classes and two subclasses: A and B. For example, the designer may introduce the IIIA wind speed class, which is related to the turbulent flow length, $L=150\text{m}$, and 15m/s turbulence intensity $I_{15}=0.18$. The turbulence intensity, I , is equal to $I=I_{15}*(2+15/U_{mean})/3$ or $I=I_{15}*(3+15/U_{mean})/4$ if the class is IIIB. The yearly mean wind speed is determined with the analyzed wind conditions and the derived Weibull distribution shape, k , and scale, A , factors, according to the empirical equation (Manwell et al., 2009, p. 59):

$$U_{mean} = A^k \sqrt[0.568 + 0.433/k]{} \quad (2.88)$$

2.4.2 Trailing edge noise

The trailing edge noise is emitted due to the interaction of the naturally turbulent flow, which is passing on both suction and pressure sides of the trailing edge of the airfoil when the flow transforms into wake within the boundary layer of the airfoil.

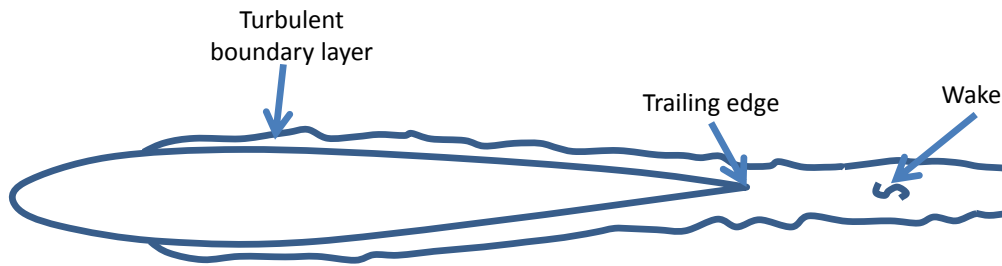


Figure 2.8: Trailing edge noise formation (Fuglsang and Madsen, 1996)

For an individual blade element, the trailing edge sound pressure level is determined with:

$$L_{pm}^{TE} = K + 10 \log(M^5 \delta^* dr / r^2) \quad (2.89)$$

where

$K=128.5$ dB is the empirical constant based on the model calibration done by Brooks et al. (1989)

M is the Mach number for the blade element, see details of Equation 2.86

dr is the section length;

r – the distance from the source of trailing edge noise to the receiver, which is equal to the blade span distance, as the noise emission investigations are carried out for the rotation centre at the receiver point;

δ^* is the thickness of the boundary layer displacement which is determined with Reynolds number, Re , and the mean chord of the blade element, c_{av} , corresponding to the respective blade element:

$$\delta^* = 0.185 c_{av} Re^{-0.2} \quad (2.90)$$

The Reynolds number is attributed to the flow passing the blade element and is found as (Hansen, 2008):

$$Re = \frac{V_{rel} c}{\nu} \quad (2.91)$$

where

$\nu=15.7 \cdot 10^{-6} \text{ m}^2/\text{s}$ is the air kinematic viscosity under 300K ambient temperature

From Equations 2.89-2.91 it is possible to derive Equation 2.92 for the noise sound pressure level of the trailing edge:

$$L_{pn}^{TE} = -15 + 10 \log \left(V_{rel}^{4.8} c_{av}^{0.8} dr / r^2 \right) \quad (2.92)$$

Equation 2.92 evaluated for each blade element is summarized for the overall trailing edge sound pressure noise of N blade elements with the interference law:

$$L_p^{TE} = 10 \log \left(\sum_{i=1}^N 10^{0.1 L_{pn}^{TE}} \right) \quad (2.93)$$

It is substituted in Equation 2.82 to derive the overall noise level due to both the trailing edge and the turbulent inflow aerodynamic noise components.

3 Optimization tools

3.1 Desirability function approach for decision making

Quite often design and operation problems face an optimization task to search the maximum or minimum of the described objective function. In the case of a single objective it is straightforward as the search procedure consists of interval choices and applies various methods (like enumeration, golden section, etc.) to find the local extreme values, minimum or maximum, depending on the task.

However, many real life problems require multiobjective optimization where the optimum compromised solution shall be found for each involved function simultaneously. Problems arise as the objective goals are contradicting each other. For example, the increase of the supermarket reliability requires a bigger storage system, i.e. additional budget expenses. Therefore, the logistic system administrator faces a problem of a multiobjective search for the increased reliability but decreased expenses. The determined goals are contradicting, and the administrator has to find a compromise solution in which most likely neither the reliability parameter nor the budget expenses reach their extreme value (maximum or minimum, respectively).

In the present thesis, there are three objective functions: the aerodynamic efficiency, the relative rotor cost and the power level of the noise. The increased aerodynamic efficiency involves most likely additional rotor expenses and increased noise emissions. The optimization goal of the study is therefore to find a compromise solution for all three objectives simultaneously.

Various methods for multiobjective optimization are introduced, classified and discussed within the following subsection. The decided optimization method, the desirability function approach, is described in section 3.1.2

3.1.1 Classification of multiobjective methods

There are different methods for the simultaneous optimization of two and more objective functions. Works of Brown (1971); Cohon (1978); de Oliveira and Saramago (2010) are specifically devoted to the introduction and classification of these approaches. The article of Boulet et al. (2009) drives an understandable and simple classification which is presented here. According to Boulet et al., there are three classes of multiobjective optimization approaches.

Goal programming

The essence of the method is the minimization of the difference between the desired and actual values of the objective function:

$$f(x) = \text{goal} - \text{what can be achieved} \rightarrow \min \quad (3.1)$$

The procedure may introduce restrictions and constraints. However, the main limitation of the goal programming approach is the difficulty to create a mathematical description for function $f(x)$ which would play a role of connection between two and more objective functions and introduce a single boundary function. The procedure involves static data processing for the analysis of liaisons.

Analytic hierarchy process

The essence of the method is to divide complex tasks into smaller components which are hierarchically considered according to their significance for the final solution. Each component is attributed with possible variants, and the final solution is derived on the basis of these variants. The method is mainly used for difficult cases which contain countable (cost, time, size, etc.) and uncountable (motivation, satisfaction, etc.) parameters. However, its application is limited in cases in which all possible variants or options are unknown beforehand.

Weighted function

The method transforms the multiobjective optimization to the maximization of a single aggregated function. Each objective is assigned with respective weights in the overall optimum solution. Harrington (1965) and Derringer (1994) proposed an equation for the aggregated function which they called the desirability function. This approach is favoured, especially because it can be combined to operate with variables of different units, for example, cost and reliability, efficiency and noise level.

3.1.2 Desirability function

The general equation for the desirability function is:

$$D = \left(d_1^{w_1} \cdot d_2^{w_2} \cdot \dots \cdot d_r^{w_r} \right)^{1/\sum_{j=1}^r w_j} \quad (3.2)$$

where

w_j – the objective weight

d_j – the objective function intermediate value code representation

For the present thesis, d_i values are code representations for the aerodynamic efficiency ($j=1$), relative rotor cost ($j=2$) and noise power level ($j=3$) in the interval [0; 1]. The desirability function equation can be rewritten into Equation 3.3:

$$D = \left(\prod_{j=1}^{j=3} d_j^{w_j} \right)^{1/\sum_{j=1}^{j=3} w_j} \quad (3.3)$$

The shape of the codification functions d_j is assumed to be linear between 0 and 1 as one of the study choices equally favours the maximization of the aerodynamic efficiency and the minimization of the economy function and noise levels. This principal of coding is presented in Figure 3.1 and expressed with the linearized equations depending on the objective function in Eq. 3.4 and 3.5:

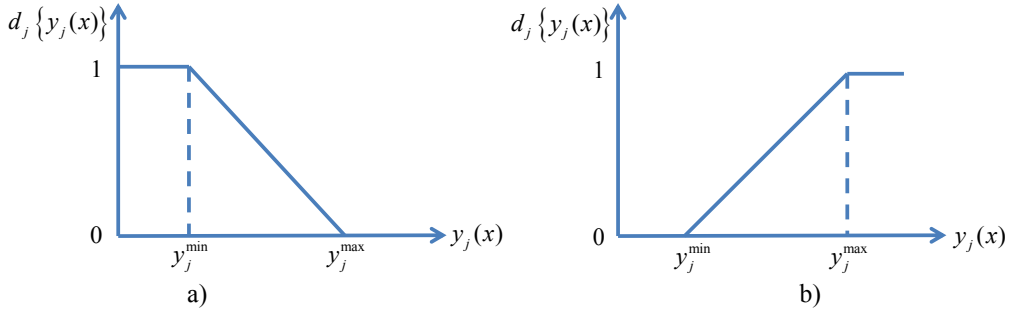


Figure 3.1: Desirability parameter coding principle for the minimization (a) and maximization (b) objectives

maximization (for the aerodynamic efficiency)

$$d_1 = \frac{y_1 - y_{1\min}}{y_{1\max} - y_{1\min}} \quad (3.4)$$

minimization (for the relative rotor cost and noise power level)

$$d_{2,3} = \frac{y_{2,3\max} - y_{2,3}}{y_{2,3\max} - y_{2,3\min}} \quad (3.5)$$

In addition, the current study develops a method for a multiobjective search procedure when the optimal blade geometry design is looked for on the constant line of one of its constructive functions corresponding to the original blade geometry. The intermediate value of the chosen function (aerodynamic efficiency, relative rotor cost or noise power level) is coded with 1 if it lies in the interval of $\pm 0.5\%$ from the respective original blade geometry measure; otherwise the code is 0. The blade measures are assumed to be insignificantly changed if they lay in the above-mentioned interval. The graphical representation of the optional codification procedure is shown in Figure 3.2:

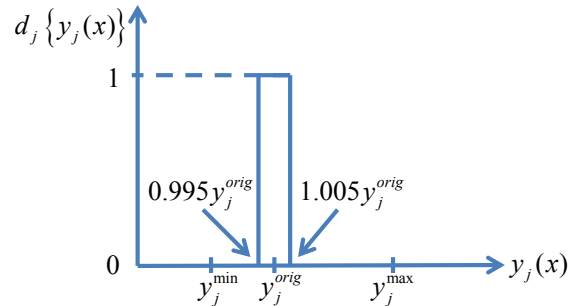


Figure 3.2: Codification principle for the optional "line" optimization

The optional optimization approach is able to simulate such multiobjective search cases, for example, as “better aerodynamic efficiency with the same blade investments as the original blade geometry” or “quieter turbine (less aerodynamic noise effect) with no reduction in the power efficiency compared to the original blade parameters”. The extended list of the investigated optimization cases is presented in section 5.4.

Figure 3.1 and Figure 3.2 introduce parameters y_j^{min} , y_j^{max} and y_j^{orig} which are the minimum, maximum and original (corresponding to the original blade geometry) values of the objective function related to the function subscript j . The search of y_j^{min} and y_j^{max} is the necessary prerequisite of the desirability function approach. The search procedure is a separate single objective optimization task. The input vector x of objective functions, which are the blade geometry parameters in this study, consists of a large number of variables. It has hence been decided to apply a differential evolution algorithm in tasks of a single objective optimization, whether it is maximization or a minimization problem. Section 3.2 reveals more details on the method of a single objective optimization based on the evolution approach.

The coding principle assigns a dimensionless measure for the objective functions. In fact, it estimates the distance of the intermediately considered value of the objective function to its global optimum (maximum or minimum, depending on the goal of the objective optimization). Therefore, the approach has the advantage of introducing the multiobjective optimization of functions with different units: aerodynamic efficiency, relative rotor cost (which are both dimensionless) and noise power level (which is measured in dB(A)).

The weight parameters w_j in Equation 3.3 are related to the decision made by the designer for the optimization of the respective objective function within the overall search procedure. The parameters are relative and scaled within a free interval which is equal for all objectives. The present study introduces a five grade scale, e.g. interval [0;5] for each weight parameter w_j .

The essence of the desirability function approach provides the opportunity for experiments. The method does not fix the optimal solution. Particular conditions of turbine installation may differ case by case compared to the initial design in terms of economy and ecology. Therefore, it is useful to have a decision making tool, such as the desirability function approach, which is affected by the particular case parameters.

3.2 Differential evolution algorithm (DEA)

The differential evolution algorithm (DEA) originating from Kenneth Price is a powerful tool for the global optimum search (Price et al., 2005). The essence of the method allows using it as a ‘black box’ which is provided with the objective function, the input vector X for the initial guess and finally achieves the optimum combination of input values for the objective function to reach its minimum or maximum, depending on the design problem. As it possesses universality, there is no need for complicate methods of tuning in particular implementation.

The background of the method lays down in the formation of population of possible candidates for the optimal solution. Each new iteration narrows down the population members’ divergence with the differential variation and crossover mutation tools until it finally reaches the true optimum when the population divergence does not bring a better solution.

The organization of DEA setup begins with a choice of number of unknown variables I_D and their bounding minimum and maximum values $X\{I_D\}_{min}$, $X\{I_D\}_{max}$ which form the initial guess interval. Each DE population consists of I_{NP} members which are recommended to be around ten times greater than the unknown variables, $I_{NP}=10 \cdot I_D$ (Price et al., 2005). At the initialization step, the input vector is combined for each population member k with a random generator within the initial boundaries:

$$X_{pop}^k = X\{I_D\}_{min} + rand_{(1,I_D)} (X\{I_D\}_{max} - X\{I_D\}_{min}) \quad (3.6)$$

The random generator $rand_{(1,I_D)}$ produces a uniformly distributed random number in the interval $[0; 1)$ for each unknown variable I_D .

The enumerative evaluation of the objective function $Y(X)$ with the initialized input vector highlights the best member of the current population Y_{best} , its index I_{best_index} and the values of the best input vector X_{best} . The best vector X_{best} has to compete against the newly generated members of the next population. The creation of new population members consists of mutation and crossover procedures.

Mutation implies the addition of scaled, randomly sampled, vector difference taken from the previous population randomly shuffled to a third vector of the previous population as well:

$$X_{mut}^k = X_0 + F(X_1 - X_2) \quad (3.7)$$

Different strategies of DEA introduce individual definitions for the base vector X_0 and factor F in equation 3.7. The following subsection 3.2.1 brings details about different DEA strategies and how the mutation procedure is carried out there. In the *best so far with jitter* strategy of DEA, which is one of investigated strategies in this thesis, the base vector X_0 is equated to the best input vector X_{best} from the previous population. The scale factor F , presented by Zaharie (2002), is a normally distributed random variable generated anew for every parameter, and is called the *jitter*:

$$F = (1 - 0.9999)rand_{(I_{NP}, I_D)} + F_{weight} \quad (3.8)$$

where the random generator $rand_{(I_{NP}, I_D)}$ is applied to every parameter of the population members, and F_{weight} is a scale factor. The scale factor has a positive real value which controls the rate of population development. According to Price et al. (2005), the effective values of the scale factor are not greater than 1.

The mutation procedure is complemented with a crossover recombination of the mutated population. The essence of the crossover is to build the final trial vector out of two vectors: the mutated and the previously populated. The responsible parameter is called the crossover probability C_r . The value lies in the interval $[0,1]$. For each parameter of the population, a randomly generated value from the interval $[0,1]$ is compared to the crossover probability. The new population parameter is equal to the mutant value if its respective random number is less than the crossover probability C_r ; otherwise the parameter inherits the old population value:

$$X_{pop}^{k,j} = \begin{cases} X_{mut}, & \text{if } rand_{(0,1)j} \leq C_r \\ X_{pop}, & \text{otherwise} \end{cases} \quad (3.9)$$

There are cases in which the newly generated population members may get undesirable or unrealistic values. For example, in the case of an airfoil type optimization task, the number of possible airfoils is limited to the stored ones. Some optimization problems may force the input vector X to be constrained with the initial guess boundaries. It is therefore crucial for the DEA procedure to be able to check whether the new population members are within the initial guess boundaries and correct the population if needed. The new population parameter is formed with a random divergence from the maximum boundary value if it is greater than this maximum and with a random divergence from the minimum boundary if it is less than this minimum:

$$\begin{aligned} X_{pop}^{k,j} &= X_{max}^j + rand_{[0,1]} \cdot (X_{best}^j - X_{max}^j), & \text{if } X_{pop}^{k,j} > X_{max}^j \\ X_{pop}^{k,j} &= X_{min}^j + rand_{[0,1]} \cdot (X_{best}^j - X_{min}^j), & \text{if } X_{pop}^{k,j} < X_{min}^j \end{aligned} \quad (3.10)$$

The evaluation of the objective function with the newly generated population reveals the winner of the current iteration as well as the new best member ever with the respective index and objective function value. The process of mutation and crossover with the following function evaluation and selection is continued until either the objective function reaches its goal value, *FVTR* (value to reach), or the number of considered populations exceeds the limit of $I_{itermax}$ defined by the designer. When the possible optimum solution is unknown, the parameter *FVTR* is set high, close to infinity. The DEA procedure is then designed and tuned to give converged and reliable result after $I_{itermax}$ iterations.

3.2.1 Differential evolution strategies

While the essence of DEA remains the same and consists of the formation of a new generation by adding a randomly sampled vector difference to the third vector and then crossovering it with the fourth vector, the particular way of mutation significantly differs in various strategies. The following overview tends to summarize the most applied strategies which are implemented in the present thesis, except the *best so far with jitter'* strategy described above.

Classic differential strategy

$$X_{mut}^k = X_0 + F_{weight} (X_1 - X_2) \quad (3.11)$$

where X_0 is a randomly chosen base vector; X_1 and X_2 are randomly shuffled difference vectors.

Target-to-best strategy

$$X_{mut}^k = X_{pop} + F_{weight} (X_{best} - X_{pop}) + F_{weight} (X_1 - X_2) \quad (3.12)$$

where X_{pop} stands for the previous population members; X_{best} is the best so far population member.

Per-vector-dither strategy

$$X_{mut}^k = X_0 + X_3 (X_1 - X_2) \quad (3.13)$$

where X_3 is the scale factor massive defined and varied for each vector:

$$X_3^k = (1 - F_{weight}) rand_{(I_{NP}, 1)} + F_{weight} \quad (3.14)$$

Per-parameter-dither strategy

The strategy does not diverge much from the *per-vector-dither* one; it applies a different scale factor for each parameter on the contrary to the constant scale factor for the whole vector in the latter strategy:

$$X_{mut}^k = X_0 + X_3(X_1 - X_2) \quad (3.15)$$

where

$$X_3 = (1 - F_{weight})rand_{[0:1]} + F_{weight} \quad (3.16)$$

Either-or strategy

The algorithm applies a classic differential strategy if the randomly generated number is less than $P_{mu}=0.5$ value (Price et al., 2005). Otherwise it applies the *F-K* rule: $K=0.5 \cdot (F_{weight} + 1)$, with the modified difference variation:

$$\begin{aligned} X_{mut}^k &= X_0 + F_{weight}(X_1 - X_2), \text{ if } rand_{[0:1]} < P_{mu} = 0.5 \\ X_{mut}^k &= X_0 + K(X_1 + X_2 - 2X_3), \text{ otherwise} \end{aligned} \quad (3.17)$$

where X_3 , as well as X_1 and X_2 are randomly shuffled vectors of the previous population.

Described DEA strategies have their own convergence possibilities which are tested in section 5.3 for the particular problem of blade geometry parameter optimization.

4 Initial information of the case study

4.1 WindPACT 1.5 MW wind turbine

WindPACT 1.5 MW wind turbine data is used for the verification of the blade shape optimization technique. The WindPACT 1.5 MW turbine design came upon the Wind Partnership for Advanced Component Technologies project run by the National Renewable Energy Laboratory (NREL) in years 2000–2002. The main turbine components (blades, generator, etc.) were investigated for alternative designs, including their respective effect on the cost of energy (COE). The ultimate goal of the project was a possible reduction of COE by 30% compared to its existing value. Detailed information about each turbine component and the design assumptions is given in the project reports (Griffin, 2001; Malcolm and Hansen, 2002; Malcolm and Hansen, 2003; Poore and Lettenmaier, 2003; Somers, 2005).

The base design is based on a 3-bladed horizontal axis turbine. It has variable speed control with active pitch regulation. The turbine tower height is $H=84$ m, hub radius $R_{hub}=1.75$ m and the overall blade radius (tip distance from the hub center) $R=35$ m. The blade cross-sections are composed of the NREL S8xx airfoil family with modified trailing edge thickness, see Figure 4.1.

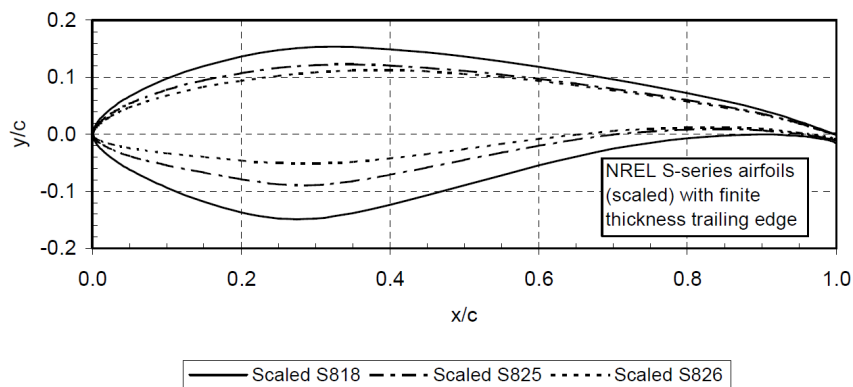


Figure 4.1: WindPACT 1.5 base design airfoils (Malcolm and Hansen, 2002)

The investigated part of the blade with constantly descending chord and increasing twist angle is presented in Figure 4.2. It is chosen instead of the full blade span because of the curve fitting problem arising on the optimization stage of the thesis, see later in section 4.2. The eliminated part of the blade does not contribute much to the overall aerodynamic efficiency, forces and torques. It is assumed to evolve from the cylindrical shape in the hub connecting the cross-section to the root section of the investigated part. Table 4.1 and Figure 4.3 show the chord, twist and airfoil type distributions for the investigated part of the WindPACT 1.5 MW turbine blade.

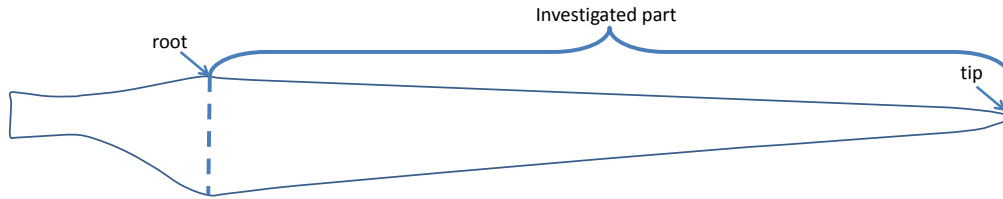


Figure 4.2: Investigated part of wind turbine blade with introduced definitions

Table 4.1: Chord, twist and airfoil distributions along the blade

R, m	Chord, m	Twist, deg	Airfoil
7.875	2.72	79.5	S818
9.625	2.64	80.9	S818
11.375	2.52	82.4	S818
13.125	2.39	83.9	S818
14.875	2.27	85.4	S818
16.625	2.14	86.6	S825
18.375	2.02	87.4	S825
20.125	1.90	87.9	S825
21.875	1.77	88.3	S825
23.625	1.65	88.8	S825
25.375	1.53	89.2	S825
27.125	1.41	89.5	S825
28.875	1.30	89.6	S825
30.625	1.18	89.7	S826
32.375	1.07	89.8	S826
34.125	0.96	89.9	S826

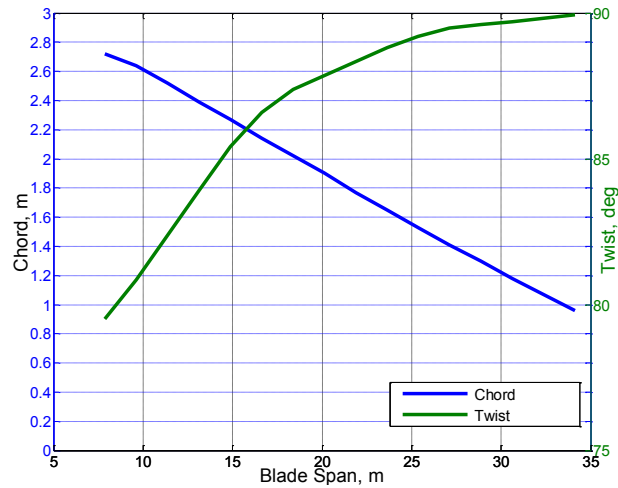


Figure 4.3: Chord and twist distribution along the blade

The work of Perfiliev et al. (2013b) presents the validation of the BEM based aerodynamic analysis tool against the CFD performance simulation of the original and modified WindPACT 1.5 MW turbine blade. The conical calculation domain with 120 degrees periodicity and 2.5 million elements, see Figure 4.4, was tested with grid independency analysis on the original blade geometry. Incompressible RANS $k-\omega$ SST turbulence model was chosen to simulate the wind blade performance.

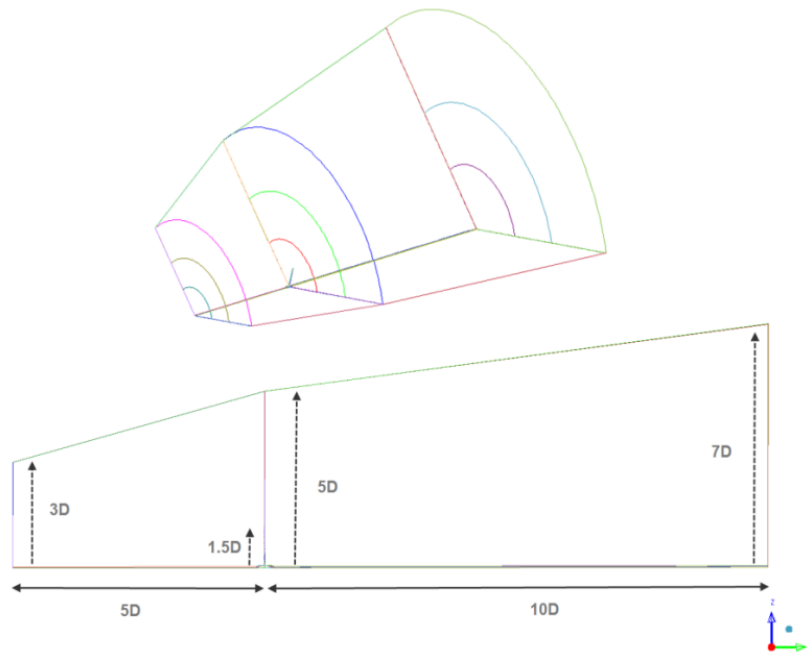


Figure 4.4. Computational domain for CFD analysis (Perfiliev et al., 2013b).

The results showed divergence of the aerodynamic efficiency obtained with BEM and CFD methods; however, a clear correlation was noted in the investigated cases of wind blade geometries. The difference is explained with the empirical and semi-accurate characterization of lift and drag properties of the airfoils as well as with the turbulent nature of the wind flow, which is not accounted in the BEM approach. However, the main advantage of the BEM is recognized in the low CPU time required for the analysis; dramatically lower than for CFD analysis.

4.2 Chord, twist and airfoil distribution boundaries

The DE algorithm requires the introduction of initial boundary intervals for variable parameters, within which the optimal solution might be positioned. In the case of blade geometry optimization, the task is to describe the chord, twist and airfoil type

distributions along the blade with a set of numerical parameters. The following is the description of the assumed variable parameters for the distributions.

The wind blade chord distribution for the investigated part is close to linear, see Figure 4.3. The linear equation for the chord distribution in Equation 4.1

$$c = a_{ch}r + b_{ch} \quad (4.1)$$

can therefore describe the family of similar distributions while varying a_{ch} and b_{ch} parameters. The mentioned parameters are included in the list of DEA optimization input variables. To simplify the dialog with the designer, the parameters a_{ch} and b_{ch} are defined with auxiliary inputs of the bounding minimum and maximum chord length of the root blade section, related to the initial blade chord with multipliers.

Figure 4.5 shows the default optimization boundaries for chord distribution set within the program.

Multipliers $m_{ch1}=1.1$ and $m_{ch2}=0.9$ to the initial root chord length determine the minimum and maximum boundary for the parameters a_{ch} and b_{ch} . The values of multipliers are assumed to derive a small enough deviation of the newly designed blade from original geometry, due to the economy model limitations, which cannot take into account the production technology modification but only the difference in the material usage.

$$a_{ch}^{\min} = \frac{c_0 m_{ch1} - c_{end} m_{ch2}}{r_0 - r_{end}} \quad (4.2)$$

$$a_{ch}^{\max} = \frac{c_0 - c_{end}}{r_0 - r_{end}} \quad (4.3)$$

$$b_{ch}^{\min} = c_0 m_{ch2} - r_0 a_{ch}^{\max} \quad (4.4)$$

$$b_{ch}^{\max} = c_0 m_{ch1} - r_0 a_{ch}^{\max} \quad (4.5)$$

The twist distribution of the initial blade geometry as well as the typical blade, see Figure 4.3, is not linear, and a similar approach as with the chord distribution cannot be implemented. The first guess when trying to approximate the distribution with common power, exponential or logarithmic functions does not result in a good agreement. Therefore, the proposed approach uses the linear addition $a_{tw}(r-r_0)+b_{tw}$ for the initial distribution function $f_I(r)$, which is tabulated in Table 1.

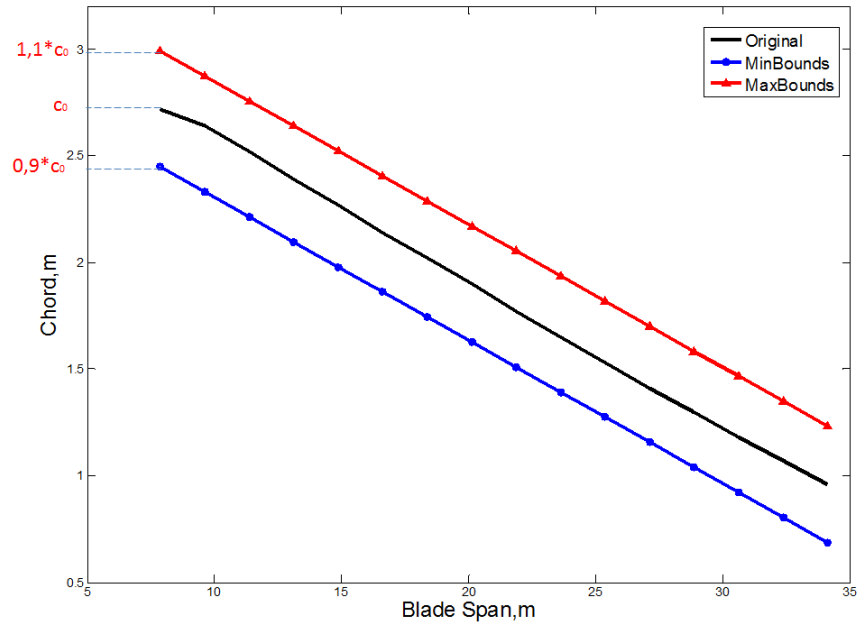


Figure 4.5: Optimization search domain for chord distribution

The resulting function $f_2 = f_1 + a_{tw} \cdot (r - r_0) + b$ is able to describe the family of twist distributions with variable parameters a_{tw} and b_{tw} , which belong to DEA optimization variables. The twist angle value for some blade cross-sections may exceed the 90 degree range. It is not practical to have a twist over 90 degrees as the summarized lift and drag force will point in the opposite way of the design direction of rotation. Therefore, the values of the present twist distribution function f_2 shall be limited to 90 degrees. Figure 4.6 presents the default boundaries for the considered minimum and maximum twist distributions. The maximum and minimum angle additions to the root twist of the initial blade geometry set by the designer. The default values are: $b_{tw}^{\max} = 0$ deg; $b_{tw}^{\min} = -5$ deg. The value of the parameter a_{tw} lies within the interval $[0; (b_{tw}^{\max} - b_{tw}^{\min}) / (r_{end} - r_0)]$, where r_{end} and r_0 are the span positions of the tip and root blade sections.

The airfoil types, their respective aerodynamic characteristics and the (x, y) cross-section coordinates are stored in the collected database. Table 4.2 shows the list of the collected airfoils with respective references. The database consists of fifteen airfoils commonly applied in the wind turbine industry. Each airfoil is coded with an integer number from one to fifteen and is referred to the list of DEA input variables within the optimization procedure. There is a possibility to avoid the airfoil type modification, which reduces the CPU time and enhances the convergence of DEA results dramatically.

The author's publications (Perfiliev et al., 2013a; Perfiliev and Backman, 2013a) present the evolution of the methods for the description of chord and twist variations with their own optimization objectives.

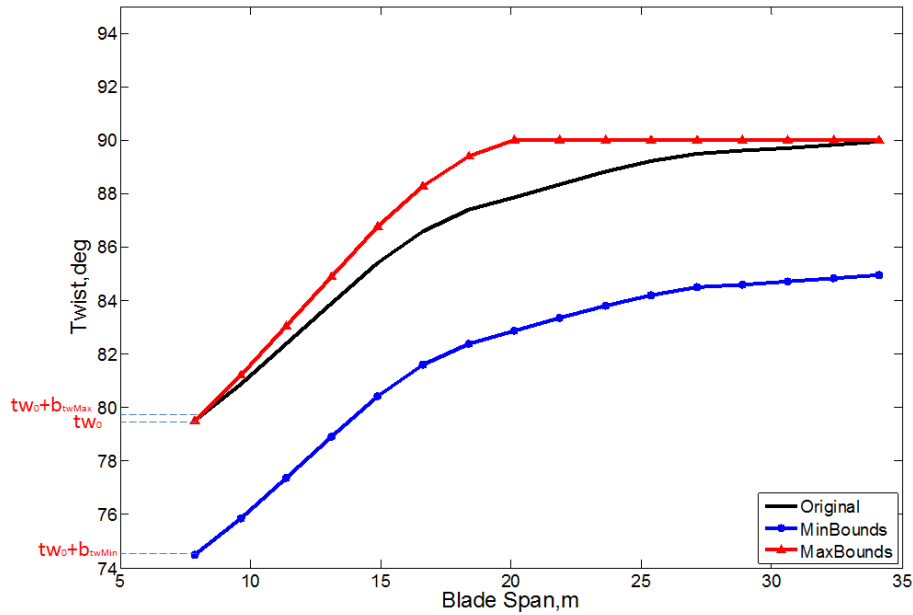


Figure 4.6: The family of twist distributions

Table 4.2: The list of collected airfoils

Airfoil name	Reference
S809	(Bertagnolio et al., 2001)
S818	(Malcolm and Hansen, 2002)
S825	(Malcolm and Hansen, 2002)
S826	(Malcolm and Hansen, 2002)
NACA63215	(Bertagnolio et al., 2001)
NACA63415	(Bertagnolio et al., 2001)
FX66S196V1	(Bertagnolio et al., 2001)
NACA65421	(Bertagnolio et al., 2001)
NACA65415	(Bertagnolio et al., 2006)
NACA64421	(Bertagnolio et al., 2006)
NACA64415	(Bertagnolio et al., 2006)
NACA63421	(Bertagnolio et al., 2001)
NACA63418	(Bertagnolio et al., 2001)
NACA63221	(Bertagnolio et al., 2001)
NACA63218	(Bertagnolio et al., 2001)

5 Methodology results

5.1 Optimal tip speed ratio and pitch angle

The aerodynamic efficiency of a variable speed pitch regulated wind turbine is dependent on the tip speed ratio λ and the initial mount pitch angle p . It is therefore crucial to find the proper tip speed ratio and pitch angle combination to maintain the maximum aerodynamic efficiency in the range between the cut-in and the rated wind speeds.

The WindPACT 1.5 MW blade geometry has been studied with the aerodynamic analysis procedure described in section 2.1 with a variable tip speed ratio and pitch angle. The typical behaviour of the aerodynamic efficiency for a step by step changing tip speed ratio and variable pitch angle is presented in Figure 5.1.

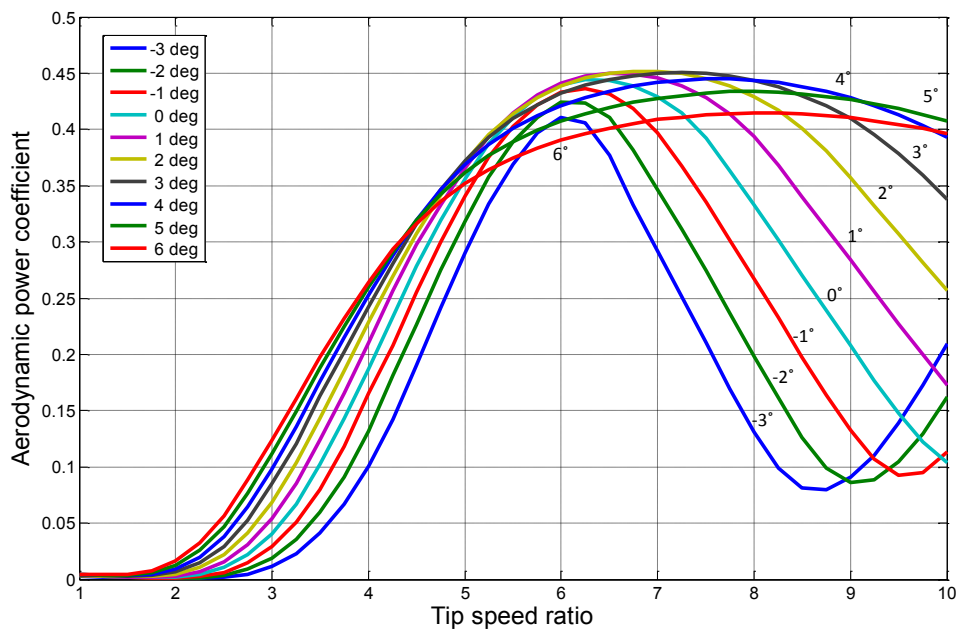


Figure 5.1: WindPACT 1.5 MW turbine aerodynamic efficiency versus tip speed ratio for different pitch angles

The search for the optimal tip speed ratio and pitch angle combination is a multiobjective optimization task with two unknown parameters. The differential evolution algorithm, described in section 3.2, has been set up to solve the problem with the intent to achieve the maximum aerodynamic efficiency.

Figure 5.2 demonstrates the convergence history for the search procedure as well as the considered population members and objective function, aerodynamic efficiency, value.

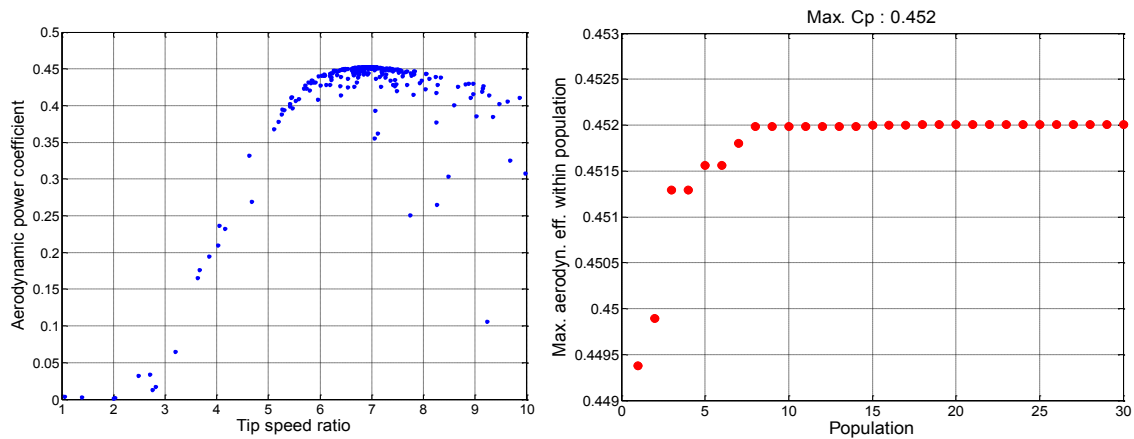


Figure 5.2: Differential evolution algorithm convergence results

At approximately the fifteenth iteration (see Figure 5.2), the solution becomes stable. The combination of the optimal tip speed ratio and pitch angle which brings the maximum aerodynamic efficiency for WindPACT 1.5 MW turbine is $\lambda_{opt}=6.9$ and $p=2$ deg. The obtained value of the aerodynamic efficiency for the initial blade geometry is $C_p=0.4519$. The received optimal tip speed ratio is close to that reported by Malcolm and Hansen (2002, p. 17), $\lambda_{opt}=7$, which is an additional partial validation of a BEM based aerodynamic tool.

The found combination values of the tip speed ratio and pitch angle are fixed for further investigations and optimization problems, to shorten the extensive number of unknown variables.

5.2 Investigation of mechanic structural parameters

The mechanical procedure requires normal and tangential force distribution under extreme wind conditions. To provide these, the aerodynamic analysis was carried out in advance. The extreme wind speed was found to be five times greater than the average wind speed. The average wind speed was found with Equation 2.88 which provided the Weibull distribution parameters, scale and shape factors. The wind turbine is assumed to be theoretically installed on an island near Vaasa (Finland) with the following Weibull factors: the shape factor $k=2.15$ and the scale factor $A=8.11$ (Finnish wind atlas, 2011).

Section 2.2.1 describes the inner structure of the blade cross-section. It was shown that six different materials are used to form the blade: the gelcoat, nexus, double-bias skin,

unidirectional composite, core material and lining. The mechanical procedure considers four materials: all excluding gelcoat and nexus, as they add a negligible contribution to the blade stiffness. The procedure is aimed to find a proper material thickness of each cross-section to withstand the structural criteria. Depending on the considered detail; AA, BB or CC (refer to Figure 2.4); the overall structural layer consists of its respective components. The mechanical procedure is a linear iterative calculation with a single unknown unidirectional composite thickness. The rest of the materials are found on the basis of a trend research of the similar size blade.

The study of Bir and Migliore (2004) for structural optimization of a 20 meter blade reveals detailed information on the thickness of the core material on different blade positions. The tabulated data is plotted in Figure 5.3 with respective trendlines of exponential functions (which are found to be reasonable for data approximation, based on the R^2 correlation factor).

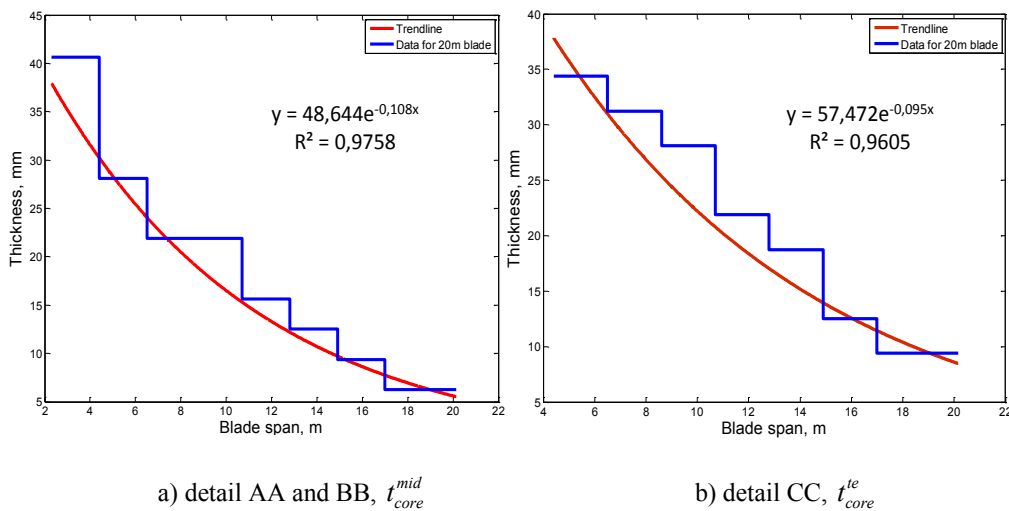


Figure 5.3: Core material thickness for blade details AA, BB and CC based on a study of Bir and Migliore (2004)

Consulting with various industrial parties allowed Bir and Migliore to derive an empirical relationship for the double-bias laminate thickness depending on the blade outer construction, i.e. the biggest chord length:

$$t_{db} = \max(0.38c_0 m_{ratio}, m_{db} t_{db}^{ply}) \quad (5.1)$$

where m_{ratio} is the minimum double-bias-laminate-to-panel-width ratio and m_{db} the minimum number of double-bias plies. Both parameters are set by the designer, and according to Bir and Migliore (2004), have in this thesis the default values 0.0025 and 3, respectively. The multiplier $0.38c_0$ is the maximum width of the blade panel

between structural webs, i.e. the length of cross-sectional detail BB, which is located between 12 and 50 percents of the chord, see Figure 2.4 for reference.

The lining material thickness is equal for the entire blade structure and is 4.07 mm. The value is based on the same study by Bir and Migliore.

The mechanical procedure carried out for the initial blade geometry with a safety factor $SF=2$ for the allowable design stress calculates the material. The thickness of each layer is adjusted to an integer number of respective unit plies, according to the unit ply thickness presented in Table 2.1.

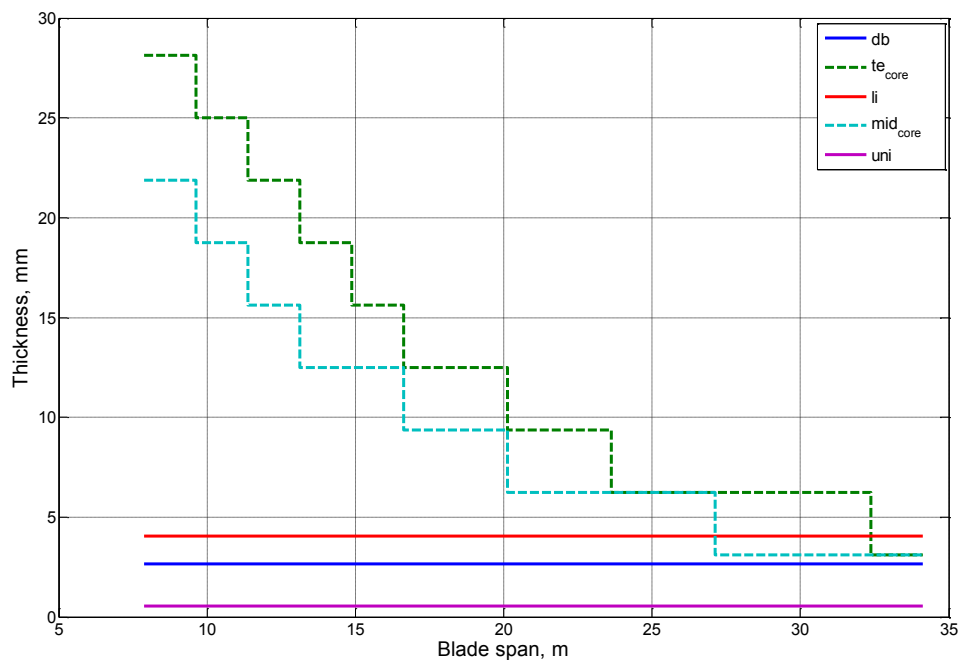


Figure 5.4: Initial WindPACT 1.5 MW blade structural layer thicknesses (db—double bias laminate, tecore—trailing edge core, li—lining, midcore—middle section core, uni—unidirectional composite)

Another value to set up for mechanical investigation and related to WindPACT 1.5 MW turbine is the static blade-tower distance which is $L=3.3$ m (Malcolm and Hansen, 2002).

The study investigated the material thickness distribution along the initial WindPACT blade which regrettably could not be compared to the other referred studies or experimental data.

5.3 Convergence capabilities of DEA strategies

The subsection investigates the convergence capabilities for the various strategies of the differential evolution algorithm described in section 3.2.1 and introduces its various parameters.

The DE algorithm is applied for the minimization and maximization problems of the current thesis. The desirability function approach requires the predefinition of minimum and maximum values for the aerodynamic efficiency, relative rotor cost, noise power level and maximum value of desirability function itself. The implemented DE algorithm allows applying only a constrained search within the initial guess boundaries, as the blade modifications shall not be large because the economy block does not assume manufacturing production changes associated with the rescaling and big divergence with the initial blade production phases. The designer may choose either to vary the airfoil type compared to the initial blade information or to leave the airfoil distribution as it is for the initial blade. The DEA search with the variable airfoil distribution is the most complicated case for the optimization procedure and requires the highest number of populations to consider for the reliable convergence. The present thesis investigates different DEA strategies' capabilities for the case of constrained optimization without airfoil type modifications. The recommended values of weight scale and crossover probability are assumed respectively: $F_{weight}=0.85$; $C_r=1$. (Price et al., 2005).

The results of various DEA strategies' investigation are summarized into Table 5.1, in which the required number of populations is presented for the final solution to be converged.

Table 5.1: Investigation of the convergence history for different optimization tasks and DE strategies. The number of populations until the results convergence.

Strategy	Aerodynamics		Economy		Noise		Desirability
	Min	Max	Min	Max	Min	Max	Max
Classic DE	>350	>350	215	>350	>350	25	>350
Target-to-best	102	>350	>350	300	177	25	>350
Best-so-far with jitter	155	250	160	163	120	25	250
Per-vector-dither	290	200	260	270	220	30	200
Per-parameter-dither	>350	260	>350	230	330	45	>350
Either-or	255	340	300	135	240	65	280

Based on the DEA strategy investigation, the *best-so-far with jitter* strategy is chosen for further implementation in the blade optimization task. The number of populations to consider in the case of not included airfoil modification is limited to 350, and in the case of airfoil modification included, it is limited to 500.

5.4 Desirability function sensitivity analysis

The investigation of the original blade geometry revealed the values for the aerodynamic efficiency, $C_p=0.4519$, the relative rotor cost, expectedly, $C_{rotor}=1$, and the noise power level, $L_w=111.7$ dB(A).

The first series of the desirability function weight variation is carried out to test the reliability of the optimization and decision making approach. The multiobjective not constrained search results are summarized in Table 5.2 and Table 5.3 for the cases of not-included and included initial blade airfoil type modification, respectively.

Table 5.2: Sensitivity analysis for desirability function with not included airfoil modification

Case	w_{Cp}	w_{Crotor}	w_{Lw}	C_{pOpt}	$C_{rotorOpt}$	L_{wOpt}	D	Comments
1	5	0	0	0.4526	0.989	112.8	1.00	Best aerodynamic efficiency (AE)
2	0	5	0	0.3737	0.682	128.9	1.00	Best relative rotor cost (RRC)
3	0	0	5	0.4077	1.182	107.7	1.00	Best noise power level (NPL)
4	1	1	1	0.4477	0.881	115.4	0.72	Equal desire for all objectives
5	1	3	5	0.4511	0.923	114.0	0.66	NPL opt. privilege
6	1	5	3	0.4422	0.842	117.1	0.66	RRC privilege
7	1	5	5	0.4453	0.861	116.2	0.65	Opt. for RRC and NPL
8	5	1	5	0.4515	1.035	110.6	0.83	Opt. for AE and NPL
9	5	3	1	0.4447	0.856	116.3	0.80	AE privilege
10	5	5	1	0.4368	0.817	118.5	0.78	Opt. for AE and RRC

Table 5.3: Sensitivity analysis for desirability function with included airfoil modification

Case	w_{Cp}	w_{Crotor}	w_{Lw}	C_{pOpt}	$C_{rotorOpt}$	L_{wOpt}	D	Comments
1	5	0	0	0.4568	1.020	112.8	1.00	Best aerodynamic efficiency (AE)
2	0	5	0	0.2669	0.674	128.9	1.00	Best relative rotor cost (RRC)
3	0	0	5	0.2907	1.175	107.7	1.00	Best noise power level (NPL)
4	1	1	1	0.4529	0.870	115.5	0.73	Equal desire for all objectives
5	1	3	5	0.4472	0.924	113.7	0.67	NPL opt. privilege
6	1	5	3	0.4448	0.839	116.8	0.67	RRC privilege
7	1	5	5	0.443	0.856	116.1	0.65	Opt. for RRC and NPL
8	5	1	5	0.4539	1.029	110.5	0.84	Opt. for AE and NPL
9	5	3	1	0.4388	0.832	117.2	0.81	AE privilege
10	5	5	1	0.4315	0.787	119.8	0.80	Opt. for AE and RRC

The designer gets the best solutions for the desired weights reflecting various scenarios. Finally, the chosen weight combination is attributed with objective function values and respective input variables describing the chord, twist and airfoil distributions along the

optimized blade. The thesis prerequisites do not introduce any particular technical, economic or environmental scenario, and therefore, based on the sensitivity analysis results brought for the WindPACT 1.5 MW turbine, the choice for the best aerodynamic efficiency is taken for the case of optimization with not-included airfoil modification, i.e. case number one in Table 5.2, and equal optimization desire for aerodynamic efficiency and noise power level, i.e. case number eight in Table 5.3, which are both marked with grey colour.

The distributions of chord length and twist angle for the obtained blade geometries are presented in Figure 5.5 and Figure 5.6 with the respective distributions of the original geometry. The airfoil distribution for the optimized blade geometry with the modified airfoil type is presented in Table 5.4 with the original distribution for comparison.

The relative and absolute differences achieved in the aerodynamic efficiency, relative rotor cost and noise power level with optimized geometries compared to the initial one are summarized in Table 5.5.

The desirability approach optimization shows that the particular WindPACT 1.5 MW turbine has not been significantly improved in terms of the objective parameters. The maximum enhancement of the aerodynamic efficiency is around 0.2%, which requires simultaneously a 2.9% increase in capital investments. However, the essence of the desirability function approach as a multiobjective decision making tool was investigated and brought adequate, roughly expected, results.

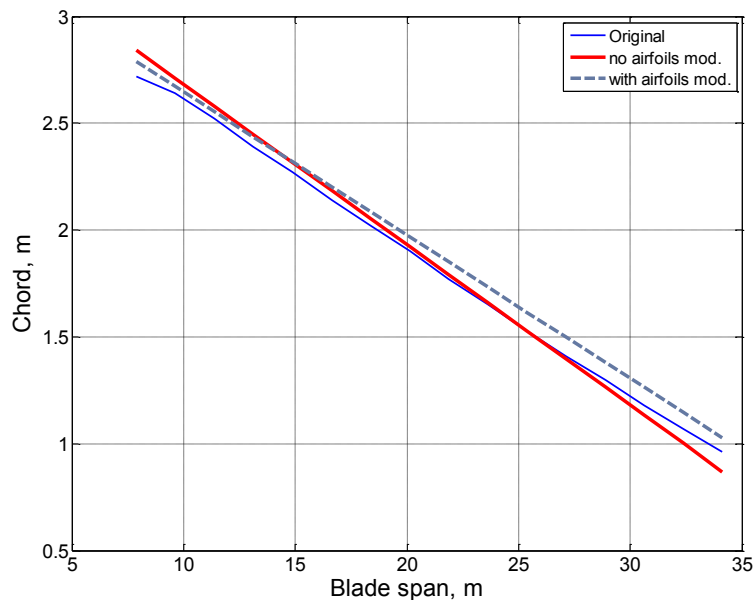


Figure 5.5: Chord distributions for original and optimized blade geometries of WindPACT 1.5 MW turbine

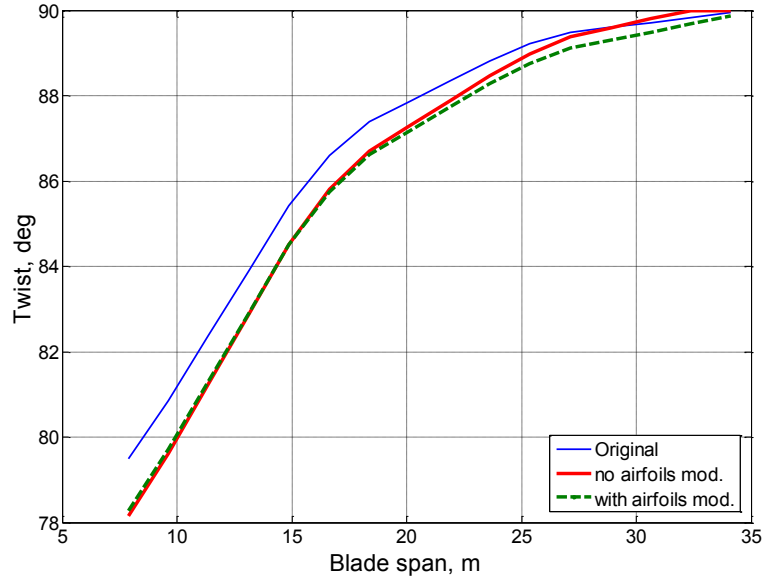


Figure 5.6: Twist distributions for original and optimized blade geometries of WindPACT 1.5 MW turbine

Table 5.4: Airfoil distribution for original and optimized blade with modified airfoils (Case 8 from Table 5.3)

Radial distance, m	Type of the blade cross section	
	Original	Mod. Airfoils
7.875	S818	NACA65421
9.625	S818	S826
11.375	S818	NACA64415
13.125	S818	S826
14.875	S818	S826
16.625	S825	NACA64415
18.375	S825	S826
20.125	S825	S826
21.875	S825	S826
23.625	S825	S825
25.375	S825	S826
27.125	S825	S826
28.875	S825	S826
30.625	S826	S826
32.375	S826	S826
34.125	S826	NACA65415

Table 5.5: Results of the chosen cases based on the desirability approach optimization for not-constrained multiobjective search

	origin (O)	no airfoil mod.			with airfoil mod.		
	value	value	absolute diff. to O, % or dB(A)	relative diff. to O, %	value	absolute diff. to O, % or dB(A)	relative diff. to O, %
$C_p, \%$	45.19	45.26	0.07	0.15	45.39	0.20	0.44
C_{rotor}	1	0.989	-1.10	-1.11	1.029	2.90	2.82
$L_w, \text{dB(A)}$	111.7	112.80	1.10	0.98	110.50	-1.20	-1.09

The second investigation introduced “line” constraints for constructive objective functions (aerodynamic efficiency, relative rotor cost and noise power level), meaning that the optimal solution was looked for on the line of the original value of the respective objective function within the allowable divergence interval $\pm 0.5\%$ (see section 3.1.2 for details), presenting the constrained multiobjective optimization. The results are shown in Table 5.6 and Table 5.7 for the not-included and included airfoil modification cases.

Table 5.6: Desirability function investigation for "line" constrained search without original airfoils modification.

Case	w_{Cp}	w_{Crotor}	w_{Lw}	C_{pOpt}	$C_{rotorOpt}$	L_{wOpt}	D	Comments
1	1	5	0	0.4497	0.902	114.7	0.62	Original AE line and best RRC
2	1	0	5	0.4497	1.156	108.6	0.96	Original AE line and best NPL
3	5	1	0	0.4525	0.995	112.5	1.00	Original Crotor and best AE
4	0	1	5	0.4510	1.005	111.4	0.85	Original Crotor and best NPL
5	0	5	1	0.4522	0.979	112.2	0.47	Original NPL and best RRC
6	5	0	1	0.4524	1.044	112.2	1.00	Original NPL and best AE

The potentially interesting variants of the modified blade geometry in Table 5.6 are marked with grey colour. They represent the hypothetical scenarios in which the modified blade design possesses the original aerodynamic efficiency or relative rotor cost or noise power level and improves one of the rest parameters. The obtained results show adequate desirability function behaviour and bring beneficial opportunities for blade geometry modifications.

The chord and twist distributions for the picked up choices are presented in Figure 5.7 and Figure 5.8 in comparisons with original geometry distributions.

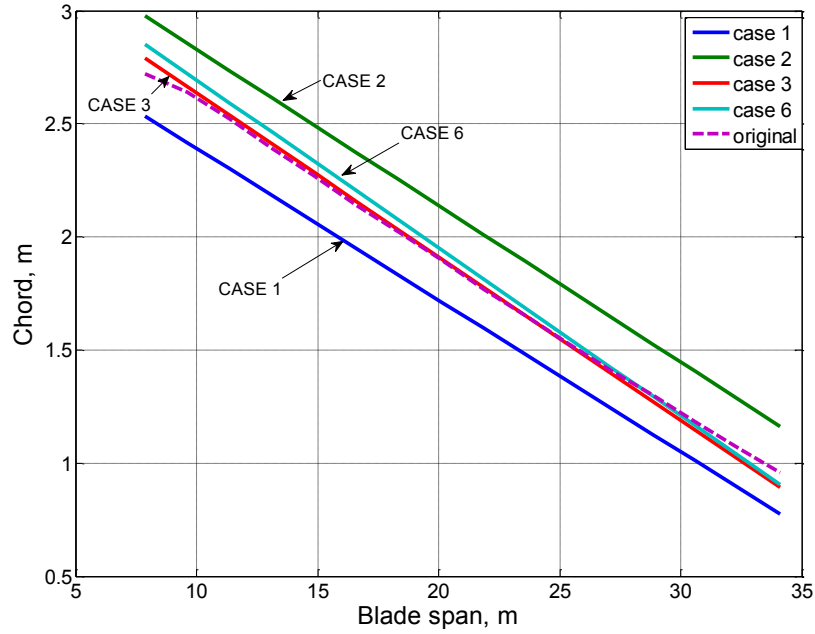


Figure 5.7: Chord distributions for the original and “line” constrained optimized blade geometries of WindPACT 1.5 MW with not-included airfoil modifications

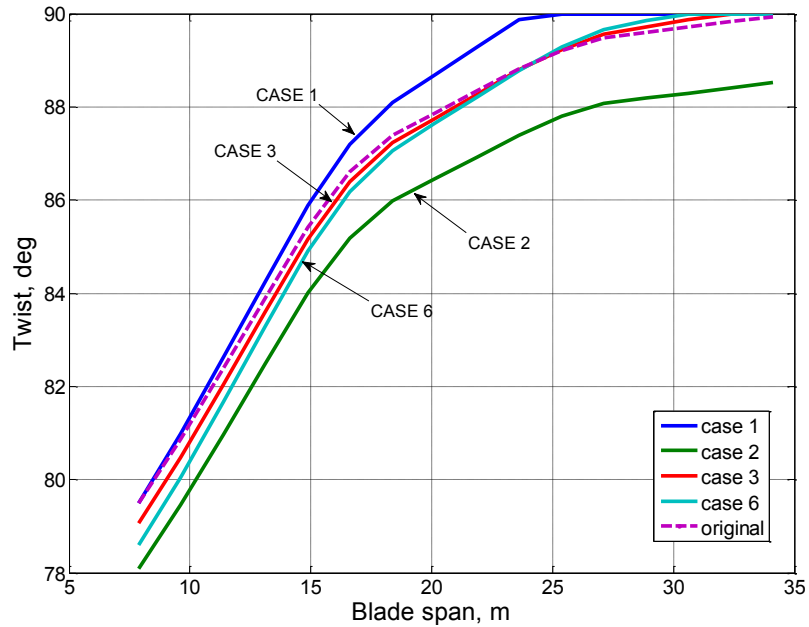


Figure 5.8: Twist distributions for the original and “line” constrained optimized blade geometries of WindPACT 1.5 MW with not-included airfoil modifications

The same “line” constrained multiobjective search with the included possibility of airfoil type modifications revealed additional blade geometry scenarios. The practise required increasing the considered number of DE populations up to 1500 to receive converged results. However, the results of constrained aerodynamic efficiency couldn't present adequate values and can't be reliable. The reason of such behaviour is under investigation, but clear reason can't be presented yet. Table 5.7 presents the results of the investigation. The chord and twist distributions along the blade span for the picked up cases (marked with grey in Table 5.7), which show the potential benefit from technical, economic or environmental perspectives are presented in Figure 5.9, Figure 5.10 and Table 5.8.

Table 5.7: Desirability function investigation for "line" constrained search with possibility of airfoils modification.

Case	w_{Cp}	w_{Crotor}	w_{Lw}	C_{pOpt}	$C_{rotorOpt}$	L_{wOpt}	D	Comments
1	1	5	0	0.3143	0.957	116.1	0.00	Original AE line and best RRC
2	1	0	5	0.3360	0.977	115.4	0.00	Original AE line and best NPL
3	5	1	0	0.4545	1.040	111.6	1.00	Original Crotor and best AE
4	0	1	5	0.3939	1.005	111.2	0.86	Original Crotor and best NPL
5	0	5	1	0.3899	0.970	112.2	0.50	Original NPL and best RRC
6	5	0	1	0.4505	0.997	111.8	1.00	Original NPL and best AE

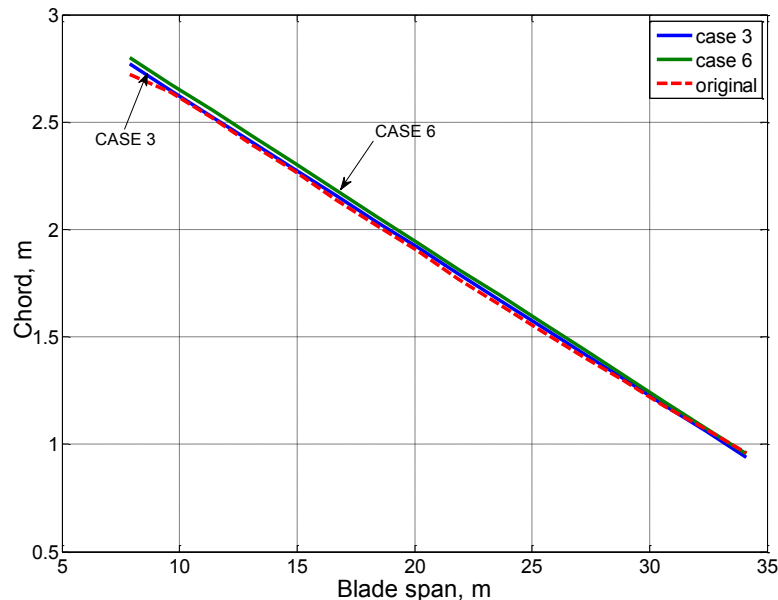


Figure 5.9: Chord distributions for original and “line” constrained optimized blade geometries of WindPACT 1.5 MW with possibility to modify the airfoil type

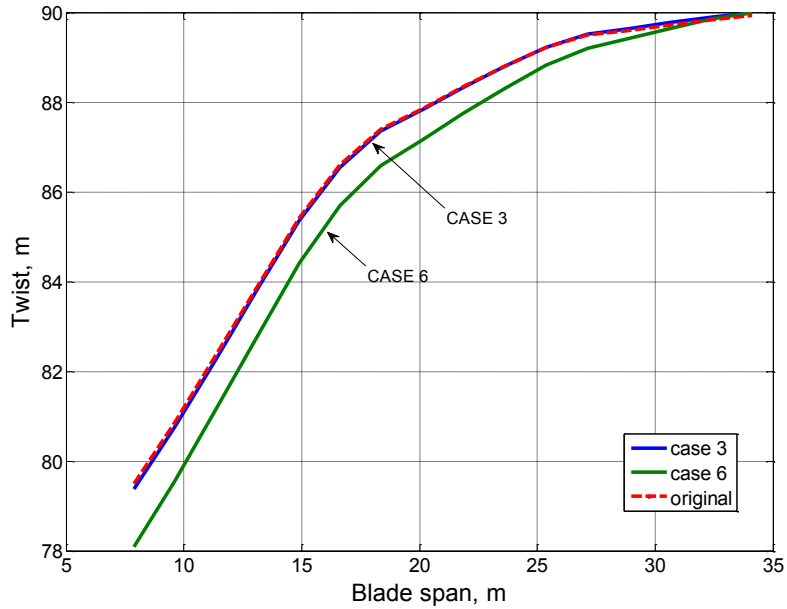


Figure 5.10: Twist distributions for original and “line” constrained optimized blade geometries of WindPACT 1.5 MW with possibility to modify the airfoil type

Table 5.8: Airfoil distribution for original and optimized blades with modified airfoils

Radial distance, m	Type of the blade cross section		
	Original	Case 3	Case 6
7.875	S818	NACA65421	NACA64415
9.625	S818	S826	FX66S196V1
11.375	S818	S826	S826
13.125	S818	NACA64415	FX66S196V1
14.875	S818	NACA64415	S826
16.625	S825	NACA64415	FX66S196V1
18.375	S825	S826	S826
20.125	S825	S826	S825
21.875	S825	S826	S826
23.625	S825	NACA64421	S826
25.375	S825	S826	S826
27.125	S825	S826	S825
28.875	S825	S826	S826
30.625	S826	S826	S826
32.375	S826	S826	S826
34.125	S826	NACA64415	NACA63415

The designer faces real life situations with different conditions of economy possibilities and noise emission factors. Depending on these, the blade design can be modified to bring the maximum proficiency, not only technical. The desirability function approach gives a universal tool for the designer to vary the attitude to respective output objectives and simulate various technical, economy and environment conditions of a particular wind turbine installation project.

6 Summary and Conclusions

Today, wind power plays a significant role in the world energy policy. Although it has a history of more than two thousand years, its development took a significant leap only during the last three decades, and wind energy asserted itself among renewable energy sources and the global energy supply system. At the current stage, the industry develops further each turbine component individually. Among the main turbine components are the tower, nacelle, generator, blades, control system and monitoring systems. The introduction section of the thesis shows that the blades constitute approximately 20–25% of the turbine overall budget, and therefore, its optimization, which is reflected with geometry and structural parameters, is a task worth the effort.

The literature review introduced a range of works devoted to the blade geometry optimization problem and derived a classification of objective functions for the final decision making. The two existing generations of objectives were found to be: 1) the aerodynamic efficiency and the annual energy production and 2) the economy derivative, cost of energy, which is the measure of price per unit power produced.

The third generation objective function, which is multiobjective, was introduced within the thesis. Multiobjective optimization implies the search of compromise values for a set of objective functions. The reason for the multiobjective optimization instead of a single objective is discussed, and it was found that the turbine production and operation parameters are often contradicting each other. For example, the enhanced aerodynamic efficiency may be coupled with increased capital investments in the blade production.

The review of the suggested objective functions revealed a growing attention to environment issues related to the wind turbine operation, i.e. noise emissions. However, not enough published works were found in which noise emissions would be considered together with other objectives, for example, the cost function.

The thesis made a contribution to include the noise emission factor in conjunction with aerodynamic and economic factors. Particular objective functions were introduced in the form of aerodynamic efficiency, relative rotor cost and noise power level. The consideration of the aerodynamic efficiency in conjunction with the rotor cost instead of the commonly accepted single cost of energy investigations, derived a wider range of solutions to analyse and made the tuning process more sensitive to practical cases in which it is easier to describe the economy condition on the basis of “how much more or less the manufacturer is able to pay for a new blade design”.

To handle several objective functions simultaneously and reach a compromise solution, the review of multiobjective optimization techniques was carried out, and the weighting approach was found to be particularly suitable for implementation in the wind turbine blade geometry optimization. The desirability function, which presents the weighting technique when objective functions are given their respective attitudes within the overall optimization, was chosen to form the final objective function which had to be

maximized—the maximum value is related to the best compromise values of the forming objectives.

The wind blade geometry search procedure was carried with three major blocks: 1) the presentation of initial information, boundaries and constraints; 2) analysis tools and 3) optimization tools.

The optimization objective, the maximization of the desirability function, required the pre-calculation of theoretically possible maximum and minimum values of the forming objectives— aerodynamic efficiency, relative rotor cost and noise power level.

The analysis of the existing techniques for a single objective maximization/minimization task showed the suitability of the differential evolution algorithm, as it provided the universal platform and allowed the consideration of a large number of objective function combinations. The algorithm was applied for the entire single objective search.

The analysis tools consisted of aerodynamic, mechanic, economy and noise emission parameter investigations. Due to the large number of blade geometry characteristic combinations, the analysis procedures were intended to be straightforward and consume only a small amount of the CPU time for each consideration.

The robustness of the analysis and optimization tools was showed and partially validated with a practical simulation example based on the obtained information about the test WindPACT 1.5 MW turbine theoretically installed on the island near Vaasa (Finland) with provided wind condition characteristics.

The investigation of aerodynamic loads, moment and efficiency was carried out with the Blade Element Moment method, which is found to be the industry standard as a fast and robust tool. The advanced technique for airfoil characteristics, lift and drag coefficients, was presented, which eliminated computer demanding simulations and decreased the amount of data that had to be stored. Although the presented method limits the characteristic variation only with the angle of attack and neglects their dependence on the Reynolds number, the study showed that simplification is possible for the considered large scale wind turbines. The collection of airfoil characteristics with the respective airfoil geometric data was encountered for fifteen different profiles used in the wind turbine manufacturing. With the optimization opportunities provided by the developed search procedure and tools it was possible to consider or eliminate the airfoil type variation. The previous research of the author demonstrated the validity of the chosen aerodynamic tool.

The load distribution along the blade in extreme wind conditions received with the aerodynamic analysis was introduced to the mechanical investigation procedure which for the chosen blade inner configuration allowed the computation of structural material thicknesses. The applied modelling theory considered three structural conditions which

the blade has to fulfil: 1) the ultimate strength factor, 2) buckling load and 3) maximum tip deflection.

The material thickness with the outer blade geometry parameters (chord, twist and airfoil type distributions) were taken into account in the economy analysis. The introduced economy model derived the dimensionless rotor cost based on the material consumption and the chord length. The definition of the relative rotor cost parameter allowed driving from the real monetary estimates to a dimensionless scale representation of the blade costs, and provided the designer with a suitable measure to compare the initial blade and optimized one with the percentage difference.

The wind turbine aerodynamic noise emissions, which were found as an A-band noise power level on the hub height and in the centre point of the rotation of the blades, were calculated with a semi-empirical straightforward model and were presented as an additional objective value. The fact signified the multiobjective nature of the optimization procedure.

Various strategies of the differential evolution algorithm were compared on the basis of convergence capabilities, and the *best-so-far with jitter* strategy was chosen for the following implementation in the practical analysis and optimization procedure of the WindPACT 1.5 MW blade geometry.

The optimization procedure required the pre-definition of the design tip speed ratio and mounting pitch angle. The optimal combination of parameters for the initial WindPACT 1.5 MW turbine blade geometry was found with an external search which involved the aerodynamic analysis and differential evolution algorithm with the intention to obtain the maximum aerodynamic efficiency. The found values of the tip speed ratio and pitch angle are respectively: $\lambda_{opt}=6.9$ and $p=2$ deg.

The investigation of the initial blade geometry revealed the values of the aerodynamic efficiency, $C_p=0.4519$, relative rotor cost, expectedly, $C_{rotor}=1$, and noise power level $L_w=111.7$ dB(A). The following desirability function sensitivity analysis obtained the results for the optimized blade geometries with respect to the designer attitude for respective weights of objective functions in the overall optimization procedure. The search domain was constrained with the linearly distributed family of chord distributions, linearly adjusted twists and limited number of possible airfoil type modifications (with respect to the collected database). The results showed the possibilities to optimize the initial blade geometry and obtain better characteristics with respect to the objectives: aerodynamic efficiency, rotor cost and noise power level. The investigated initial WindPACT 1.5 MW blade appeared to have good design characteristics, and the optimization procedure with no airfoil modification allowed to increase its original aerodynamic efficiency with roughly 0.07%, and although it came with the noise emission growth of 1.1 dB(A), the relative rotor cost could be decreased by 1.1%. The modification of the initial airfoil type distribution showed the possibility

to enhance the original aerodynamic efficiency with 0.2% and to reduce the noise power level for 1.2 dB(A), but the benefits increased the relative rotor cost by 2.9%.

The introduced optimization technique develops the novel approach for multiobjective view on the decision making related to the wind turbine blade geometry design. The final decision shall be connected to the real case situation which is described with technical, economic and environmental conditions. The approach presents the measures for each factor mentioned with their aggregating method.

6.1 Suggestions for future work

The developed methodology and tools for the wind blade geometry design are a prototype for the multiobjective optimized solution that has potential for further improvements. The assumptions introduced through the thesis are the main candidates for modification, which could make the modelling procedures closer to practice. For instance, the lift and drag characteristics of the airfoils are assumed to be independent of the Reynolds number. Considering the modification of the characteristic simulation has potential benefits.

The chord and twist distributions are expressed with linear and additive equations. Another approach for distribution descriptions found in the literature is the application of Bezier curves. The investigation of its implementation and the definition of potential benefits could make a valuable addition to the optimization approach.

The future work may be directed into the experimental validation of the proposed theoretical tools and the characteristics of the obtained optimal designs, as the validation here is limited.

The development of a user friendly environment which would present the methodology of the wind blade design and optimization may attract people to use the approach and program. An attempt to develop such a graphical user interface has been taken by the author, and the results are presented in Appendix A.

References

- Airfoil coordinates catalogue (2013). *Profiles coordinates*. [Retrieved Apr. 6, 2013], url: <http://a190754.free.fr/PROFILES.PHP3>.
- AWEA standard 2.1 (1989). Procedure for measurement of acoustic emissions from wind turbine generator systems.. Washington, DC: Americal Wind Energy Association.
- Bertagnolio, F., Sorensen, N., Johansen, J., and Fuglsang, P. (2001). *Wind turbine airfoil catalogue*. Roskilde: RISO National Laboratory. RISO-R-1280(EN), 152 p.
- Betagnolio, F., Sorensen, N.N., and Johansen, J. (2006). *Profile catalogue for airfoil sections based on 3D computations*. RISO report. Roskilde: RISO National Laboratory. RISO-R-1581(EN), 74 p.
- Bir, G.S. (2001). Computerized method for preliminary structural design of composite wind turbine blades. In: *Proceedings of the AIAA/ASME wind energy symposium*, pp. 26-37.
- Bir, G. and Migliore, P. (2004). *Preliminary structural design of composite blades for two- and tree-blade rotors*. Technical report. Golden: National Renewable Energy Laboratory.
- Bossanyi, E.A. (2003). *GH Bladed vesion 3.51 user manual*. User manual. 282/BR/010, 124 p.
- Bossanyi, E.A. (2010). *GH Bladed theory manual*. Theory manual. 282/BR/009, 103 p.
- Boulet, J.-F.B., Gharbi, A., and Kenne, J.-P. (2009). Multiobjective optimization in an unreliable failure-prone manufacturing system. *Journal of quality and maintenance engineering*, 15(4), pp. 397-411.
- Brooks, T.F., Pope, D.S., and Marcolini, M.A. (1989). *Airfoil self-noise and prediction*. NASA report. National Aeronautics and Space Administration.
- Brown, A.R. (1971). *Optimum packing and depletion: the computer in space- and resource-usage problems*. London: Elsevier Publishing Company. ISBN 0 444 19588 2.
- Carcangiu, C.E. (2008). *CFD-RANS study of horizontal axis wind turbines*. PhD. thesis. Univesita Degli Studi di Cagliari.
- Cheremisnoff, N.P. (1978). *Fundamentals of wind energy*. Michigan: Ann Arbor Science Publishers, Inc. ISBN 0-250-40243-2.

- Cohon, J.L. (1978). *Multiobjective programming and planning*. Academic Press, Inc. ISBN 0 12 178350 2.
- de Oliveira, L.S. and Saramago, S.F.P. (2010). Multiobjective optimization techniques applied to engineering problems. *Journal of the brazilian society of mechanical sciences and engineering*, 32(1).
- Derringer, G.C. (1994). A balancing act: optimizing a product's properties. *Quality progress*, pp. 51-58.
- Drela, M. and Youngren, H. (2001). *XFOIL 6.9 User primer*. User manual.
- DS 412 (1983). Dansk Ingeniorforenings norm for stalkonstruktioner (Danish standard for steel constructions)..
- Fink, M.R., Schlinker, R.H., and Amiet, R.K. (1976). *Prediction of rotating-blade vortex noise from noise of non-rotating blades*. NASA CR-2611.
- Finnish wind atlas (2011). *Finnish wind atlas*. [Retrieved Aug. 5, 2011], url: <http://www.tuuliatlas.fi/fi/index.html>.
- Fuglsang, P. and Madsen, H.A. (1996). *Implementation and verification of an aeroacoustic noise prediction model for wind turbines*. RISO report. Roskilde: RISO National Laboratory. RISO-R-867(EN), 54 p.
- Fuglsang, P. and Madsen, H.A. (1999). Optimization method for wind turbine rotors. *Journal of wind engineering and industrial aerodynamics*, 80, pp. 191-206.
- Fuglsang, P. and Thomsen, K. (1998). *Cost optimization of wind turbines for large-scale off-shore wind farms*. RISO report. Roskilde: RISO National Laboratory. RISO-R-1000(EN), 31 p.
- Glauert, H. (1926). A general theory of the autogyro. *ARCR R&M*, 1111.
- Global wind energy council (2012). *Global wind report. Annual market update*. GWEC.
- Griffin, D.A. (2001). *WindPACT turbine desing scaling studies technical Area 1 - composite blades for 80- to 120- meter rotor*. Subcontractor report. Golden: National Renewable Energy Laboratory. NREL/SR-500-29492, 44 p.
- Hansen, M.O.L. (2008). *Aerodynamics of wind turbines*, 2nd edn. Sterling: Earthscan. ISBN-13 978 1 84407 438 9.
- Harrington, E.C.J. (1965). The desirability function. *Industrial quality control*, 21(10), pp. 494-498.

- Hubbard, H.H. and Shepherd, K.P. (1984). *The effects of blade mounted vortex generators on the noise from a MOD 2 wind turbine generator*. NASA.
- IEC 61400-11 (2001). Wind turbine generator systems - Part 11: Acoustic noise measurement technique.. Geneva: International Electrotechnical Commission. 88/141/CDV.
- IEC 61400-1 (2005). Wind turbines - Part 1: Design requirements.. International Electrotechnical Commission.
- IEC 61400-12-1 (2005). *Wind turbines - Part 12-1: Power performance measurements of electricity producing wind turbines*. International Electrotechnical Committee.
- Ingram, G. (2011). *Wind turbine blade analysis using the blade element momentum method. Version 1.1*. Manual. Durham University.
- Iov, F., Hansen, A.D., Sorensen, P., and Blaabjerg, F. (2004). *Wind turbine blockset in Matlab/Simulink*. Aalborg University.
- Koivuniemi, A., et al. (2011). Modeling of wind turbine performance in complex terrain using dynamic simulation. In: *Proceedings of the 15th World Multi-conference on Systemics, Cybernetics and Informatics (WMSCI)*, pp. 228-233. Orlando.
- Krohn, S., Morthorst, P.-E., and Awerbuch, S. (2009). *The economics of wind energy*. report by European Wind Energy Association. EWEA.
- Laino, D.J. (2002). *AeroDyn User's guide, version 12.50*. User manual. Salt Lake City: Windward Engineering.
- Lowson, M.V. (1993). A new prediction model for wind turbine noise. In: *Proceedings of Renewable Energy conference*. IEE.
- Madsen, H.A. (2007). *Research in aeroelasticity EFP-2006*. RISO report. Roskilde: RISO National Laboratory. RISO-R-1611(EN), 118 p.
- Madsen, H.A., et al. (2010). Validation and modification of the blade element momentum theory based on comparisons with actuator disc simulations. *Wind energy*, 13, pp. 373-389. DOI: 10.1002/we.359.
- Madsen, P.H., et al. (1990). *Expert group study on recommended practices for wind turbine testing and evaluation. 3: Fatigue loads*, 2nd edn. IEA Wind Energy Conversion Systems.
- Madsen, H.A., et al. (2006). *Research in aeroelasticity EFP-2005*. RISO report. Roskilde: RISO National Laboratory. RISO-R-1559(EN), 112 p.

- Malcolm, D.J. and Hansen, A.C. (2002). *WindPACT turbine rotor design study*. Subcontractor report. Golden: National Renewable Energy Laboratory. NREL/SR-500-32495, 82 p.
- Malcolm, D.J. and Hansen, A.C. (2003). *WindPACT turbine rotor design, specific rating study*. Subcontractor report. Golden: National Renewable Energy Laboratory. NREL/SR-500-34794, 42 p.
- Manwell, J.F., McGowan, J.G., and Rogers, A.L. (2009). *Wind energy explained. Theory, design and application*, 2nd edn. John Wiley and Sons Ltd. ISBN 978 0 470 01500 1.
- Mendez, J. and Greiner, D. (2006). Wind blade chord and twist angle optimization by using genetic algorithms. In: *Proceedings of the fifth international conference on engineering computational technology*.
- Merz, K.O. (2011). *Conceptual design of a stall-regulated rotor for a deepwater offshore wind turbine*. PhD. thesis. Trondheim: Norwegian University of Science and Technology.
- Miley, S.J. (1982). *A catalogue of low Reynolds number airfoil data for wind turbine application*. Texas: Texas A&M University. RFP-3387, 53 p.
- Moriarty, P.J. and Hansen, A.C. (2005). *AeroDyn theory manual*. Technical report. Golden: National Renewable Energy Laboratory. NREL/EL-500-36881, 35 p.
- Mortensen, N.G., et al. (2007). *Getting started with WAsP 9*. Roskilde: RISO National Laboratory, DTU. RISO-I-2571(EN), 66 p.
- Morthorst, P.E. (2009). *Wind energy - The facts. Volume 2. Costs & Prices*. EWEA.
- NREL airfoil catalogue (2013). *NREL airfoil catalogue*. National Renewable Energy Laboratory. [Retrieved Apr. 15, 2011], url: <http://wind.nrel.gov/airfoils/>.
- Oerlemans, S., Sijtsma, P., and Lopez, B.M. (2007). Location and quantification of noise sources on a wind turbine. *Journal of sound and vibration*, 299, pp. 869-883.
- Perfiliev, D. and Backman, J. (2013a). Matlab tool for multiobjective wind blade geometry optimization. In: *Proceedings of the European Wind Energy Association conference (EWEA)*. Vienna.
- Perfiliev, D. and Backman, J. (2013b). Wind turbine blade geometry optimization with differential evolution algorithm and desirability function approach. *Renewable Energy*. Submitted for publication.

- Perfiliev, D., Hamalainen, J., and Backman, J. (2013a). Robust analyzing tool for wind turbine blades coupled with multiobjective optimization. *Journal of Energy and Power Engineering*. Accepted for publication.
- Perfiliev, D., Kosmacheva, A., Backman, J., and Hamalainen, J. (2013b). Semi automated improvement of wind blade design. In: *Proceeding of the 10th European Conference on Turbomachinery Fluid Dynamics and Thermodynamics (ETC10)*. Lappeenranta.
- Poore, R. and Lettenmaier, T. (2003). *Alternative design study report: WindPACT advanced wind turbine drive train design study*. Subcontractor report. Golden: National Renewable Energy Laboratory. NREL/SR-500-33196, 556 p.
- Price, T.J. (2005). James Blyth - Britain's first modern wind power pioneer. *Wind Engineering*, 29(3), pp. 191-200.
- Price, K.V., Storn, R.M., and Lampinen, J.A. (2005). *Differential evolution. A practical approach to global optimization*. Berlin: Springer. ISBN-10: 3 540 20950 6.
- Profili software (2013). *Profili 2 download page*. [Retrieved Jan. 13, 2012], url: <http://www.profili2.com/eng/default.htm>.
- Rogers, A.L. and Manwell, J.F. (2002). *Wind turbine noise issues*. Amherst: University of Massachusetts at Amherst.
- Schlinker, R.H. (1977). Airfoil trailing edge noise measurements with a directional microphone. In: *AIAA 4th Aeroacoustics conference*. Atlanta, Georgia. DOI: 10.2514/6.1977-1269.
- Schlinker, R.H. and Amiet, R.K. (1981). *Helicopter rotor trailing edge noise*. NASA CR-3470.
- Somers, D.M. (2005). *The S827 and S828 Airfoils*. Subcontractor report. Golden: National Renewable Energy Laboratory. NREL/SR-500-36343, 54 p.
- Tadamasa, A. and Zangeneh, M. (2011). Numerical prediction of wind turbine noise. *Renewable Energy*, 36, pp. 1902-1912.
- Tangler, J.L. (2002). The Nebulous art of using wind tunnel airfoil data for predicting rotor performance. *Wind Energy*, 5(2).
- Tangler, J. and Bir, G. (2004). *Evaluation of RCAS inflow models for wind turbine analysis*. Golden, Colorado: National Renewable Energy Laboratory. NREL/TP-500-35109, 42 p.

- Tong, W. (2010). *Wind power generation and wind turbine design*. Southampton: WIT Press. ISBN: 978 1 84564 205 1.
- Wikimedia Foundation (2012). *Speed of sound*. [Retrieved May 8, 2012], url: http://en.wikipedia.org/wiki/Speed_of_sound.
- Wikimedia Foundation (2013). *Reynolds number*. [Retrieved Feb. 3, 2011], url: http://en.wikipedia.org/wiki/Reynolds_number.
- Wind power in Denmark (2013). *Wind power in Denmark*. [Retrieved Aug. 10, 2013], url: http://en.wikipedia.org/wiki/Wind_power_in_Denmark.
- Xudong, W., et al. (2009). Shape optimization of wind turbine blades. *Wind energy*, 12, pp. 781-803. DOI: 10.1002/we.335.
- Yadama, V., ed., (2007). *ASCE lectures*. American Society of Civil Engineers. [Retrieved May 7, 2011], url: <http://pas.ce.wsu.edu/CE537-1/Lectures/Rule%20of%20Mixtures.pdf>.
- Zaaijer, M.B. (2003). *Overall cost-modelling of the DOWEC lifecycle in a wind farm*. Project report. Delft: Delft University of Technology. DUWIND 2003.024, 34 p.
- Zaharie, D. (2002). Critical values for the control parameters of differential evolution algorithms. In: Matousek, R. and Osmera, P., eds, *Proceedings of 8th international conference on soft computing*, pp. 62-67. Brno.

Appendix A: Developed computer application

A1. Existing software for wind turbine design

There are several program applications related to turbine and wind station designs. Among them, there are Matlab Simulink wind turbine blockset (Iov et al., 2004), GH Bladed (Bossanyi, 2003), WAsP (Mortensen et al., 2007), AeroDyn (Moriarty and Hansen, 2005) and xFoil (Drela and Youngren, 2001).

The Matlab Simulink wind turbine blockset developed by Aalborg University in cooperation with RISO is a ready-to-use tool for the simulation of the wind turbine behaviour within scientific Simulink environment. The block consists of boxes describing the aerodynamic, electric and mechanic turbine behaviour with a range of simplified and enhanced theories for power electronics, transformers, drive shaft and various types of electric generators.

GHBladed is aimed for the turbine overall design. It includes the analysis of aerodynamic, electric and structural parameters of the turbine and station as a whole when connected to a centralized or remote grid.

The WAsP is devoted to the wind analysis and optimal turbine positioning on the chosen location. Turbine characteristics are provided by a list of collected turbines or the designer determines the power curve of the turbine and design operation conditions. The WAsP code is based on linear and interpolative studies of the wind flow behaviour. The turbine income wind is calculated using the interpolation of the wind speeds and the direction from the known surrounding locations.

AeroDyn is a set of routines provided as a product by the National Renewable Energy Laboratory (USA) for the calculation of the aerodynamics of horizontal axis wind turbines, including the turbine wakes model, blade element method, dynamic stall model and ability to analyse yawed flow conditions.

xFoil is a product of Massachusetts Institute of Technology (MIT, USA), and it is a design and analysis tool for subsonic airfoils. The analysis can be carried out for viscous (inviscid) conditions only.

The author took part in the development of Simulink/Matlab based dynamic model of variable speed pitch regulated wind turbine. The theory background, model configuration, results and validation against classic power curve approach are presented in Koivuniemi et al. (2011).

The following subsection introduces the newly developed computer tool with a graphical user interface for the analysis and multiobjective design of the wind turbine blade with respect to objective goals and particular wind conditions. The Matlab

environment is used to create a Windows application for the optimization of the wind blade shape.

A2. General introduction of the developed software

The developed software consists of blocks for the initial data provision, executions of the procedures and monitoring as well as the post-processing and analysis of the results. Figure A2.1 presents the block structure of the program.

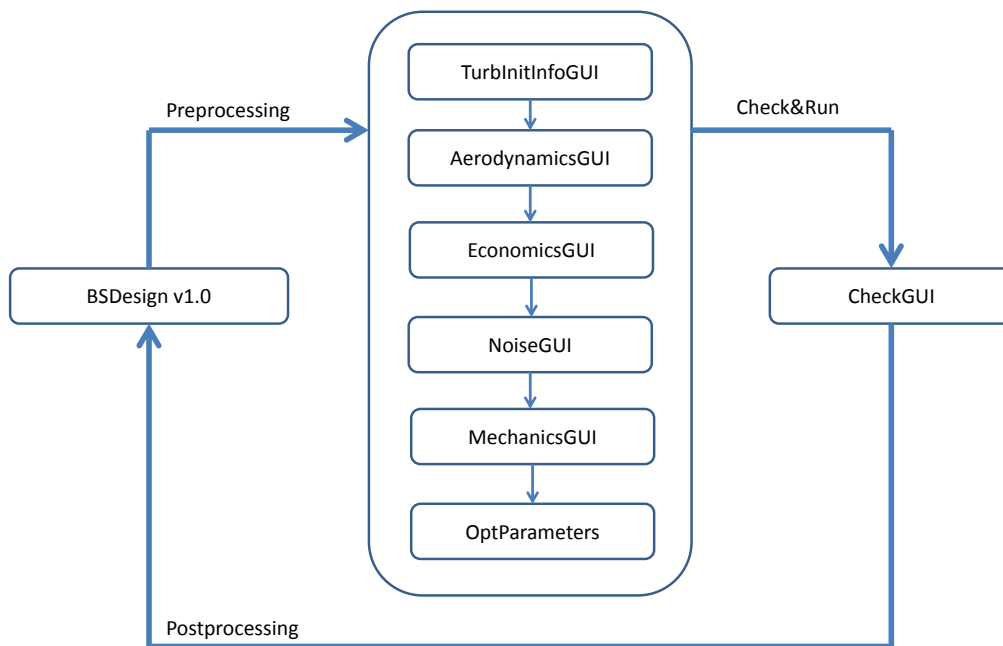


Figure A2.1: Block structure of the program

The opening screen of the program is illustrated in Figure A2.2, in which all the blocks shown in Figure A2.1 are available for access. The lower right part of the screen is reserved for the optimization results.

Original turbine and blade geometry data are provided inside the TurbInitInfoGUI window (Figure A2.3). The program shall obtain the blade and hub radius, chord, twist and airfoil type distributions along the blade span distance. The designer is allowed to enter the main blade parameters in each cross-section and select the airfoil type from a drop-down list.

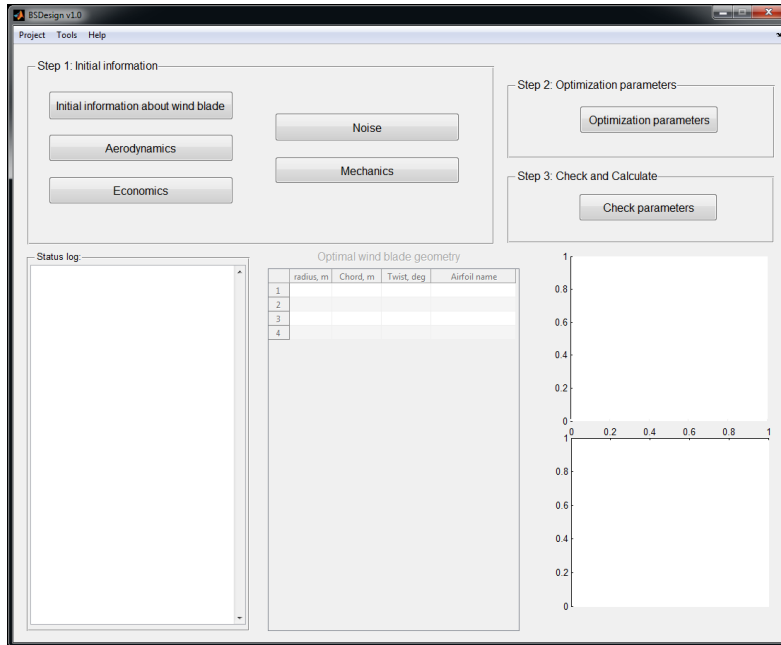


Figure A2.2: The main window of the application

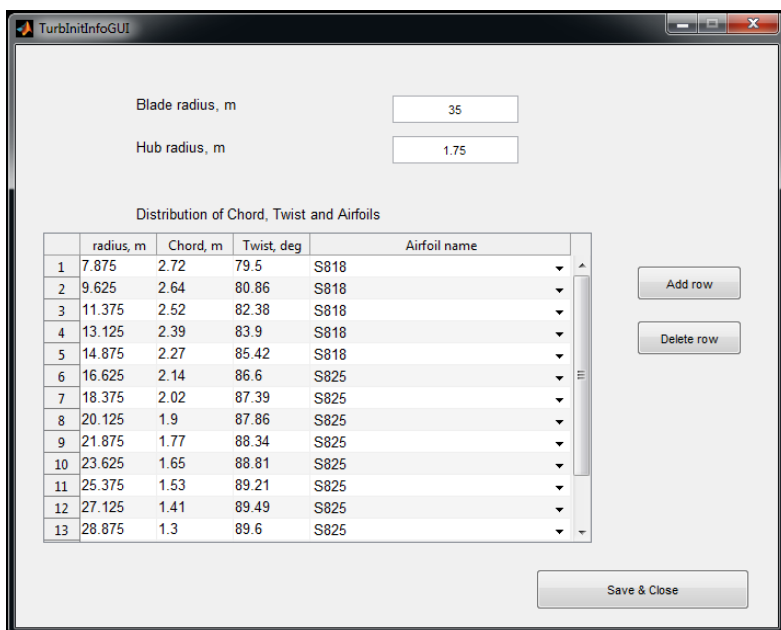
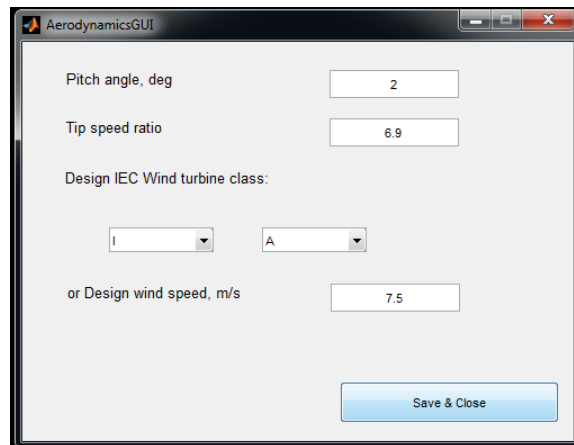


Figure A2.3: Wind blade initial geometry

The aerodynamic procedure parameters—blade pitch angle, tip speed ratio and design wind class—are entered in the AerodynamicsGUI window, see Figure A2.4. The design wind class is specified with IEC classification attributes: the number of class (from I to IV) and turbulence subclass (A or B). The design wind speed is defined afterwards with respect to the mentioned class.



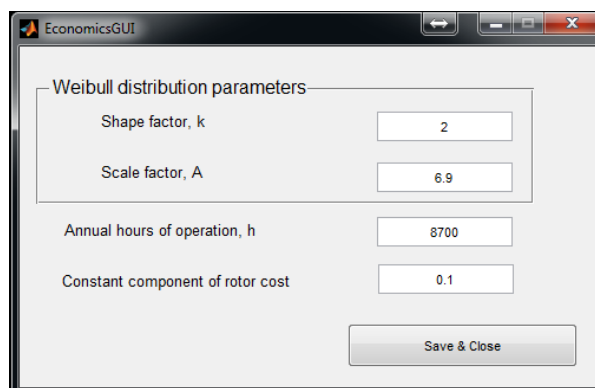
The screenshot shows a window titled "AerodynamicsGUI" with the following parameters and values:

Parameter	Value
Pitch angle, deg	2
Tip speed ratio	6.9
Design IEC Wind turbine class:	I (Class) and A (Turbulence subclass)
or Design wind speed, m/s	7.5

A "Save & Close" button is located at the bottom right of the window.

Figure A2.4: Aerodynamic conditions

To determine extreme wind speed conditions and to perform an economic procedure the designer has to provide local wind characteristics, shape and scale Weibull distribution parameters, the annual operation hours and the constant component of the relative rotor cost, which is a value from 0 to 1, and based on Xudong et al. (2009), is equal to 0.1 by default.



The screenshot shows a window titled "EconomicsGUI" with the following parameters and values:

Parameter	Value
Shape factor, k	2
Scale factor, A	6.9
Annual hours of operation, h	8700
Constant component of rotor cost	0.1

A "Save & Close" button is located at the bottom right of the window.

Figure A2.5: Economic parameters

Figure A2.6 introduces the NoiseGUI window which collects information about the turbulence flow behaviour influencing the noise emissions level: the turbulence length and turbulence intensity. If not entered, the parameters can be calculated automatically with the attributed wind class and subclass during the definition of aerodynamic parameters.

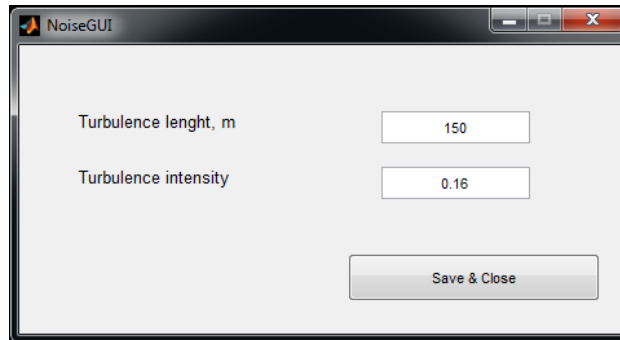


Figure A2.6: Noise parameters

The parameters introduced in MechanicsGUI, see Figure A2.7, are mechanical procedure constants: static blade-tower clearance, which is related to the particular turbine installation; safety factor for allowable extreme stresses, equal to 2 by default, based on a study of Bir and Migliore (2004) and the minimum number of double-bias plies, designed to be 3 by default, based on the same study.

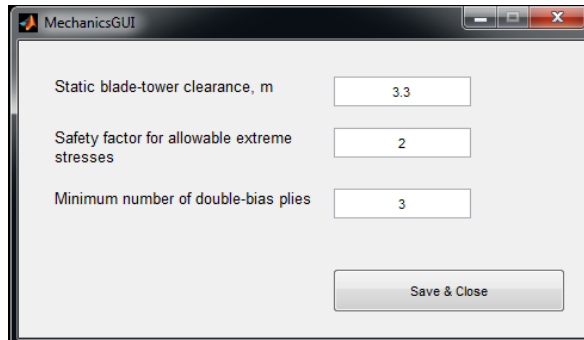


Figure A2.7: Mechanical parameters

Figure A2.8 presents the design of crucial optimization parameters: search bounds, objectives and methodology. The approach to define chord and twist variation constraints is explained in detail in section 0. The option to include or exclude airfoil type modification inside the optimization search procedure is ticked with the respective

checkbox, which increases the search dimension substantially. Desirability function weights are determined for objective functions of aerodynamic efficiency, relative rotor cost and noise power level, and they are integer numbers in a drop-down list from zero to five. The strategy method of the differential evolution algorithm can be chosen among six pre coded strategies explained in detail in section 3.2.1.

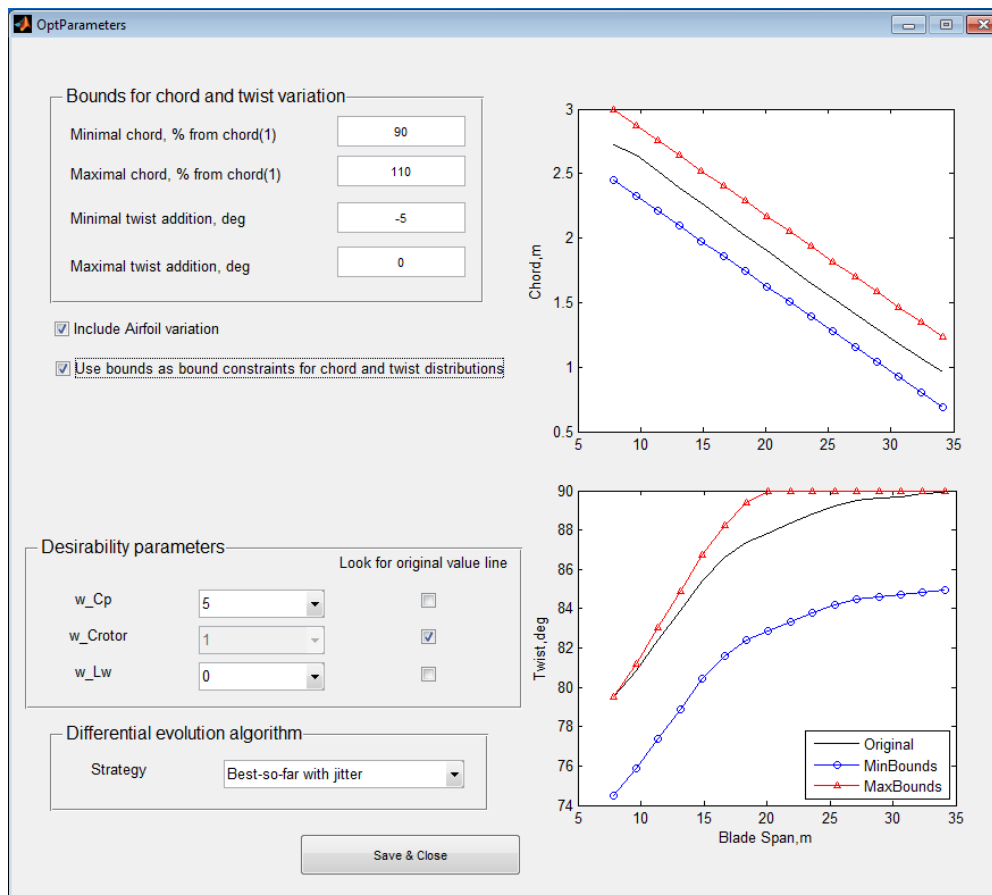


Figure A2.8: Optimization search parameters

The introduced set of initial information parameters is checked in the CheckGUI window (see Figure A2.9). The final version of parameter set is stored in a special structural file that is loaded during the analysis and optimization procedures. *Save&Run* button starts the optimization procedure: executing the analysis, search and decision making tools - described in sections 2 and 3.

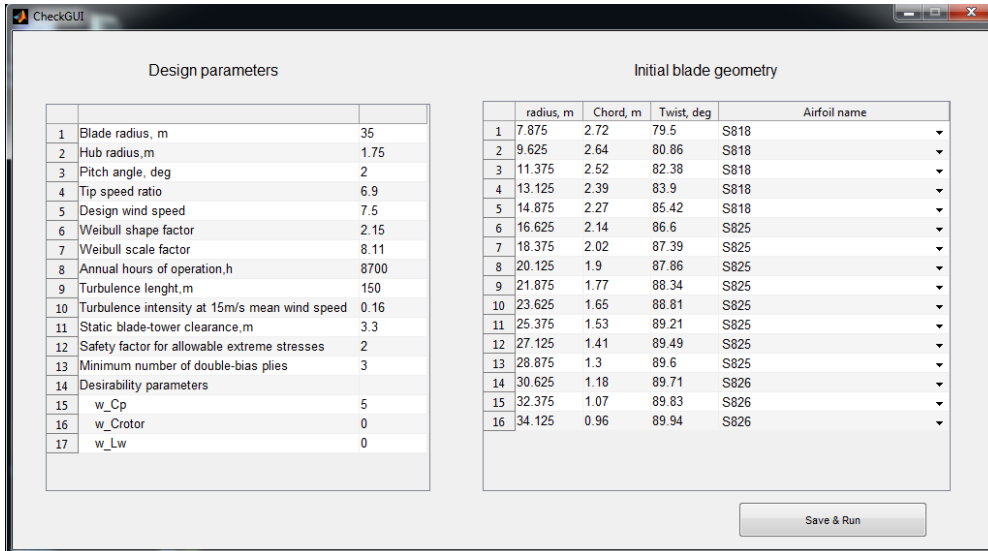


Figure A2.9: Overall parameters check and optimization procedure run

The m-files collection code listing consists of around 3500 lines. There are about 20 user inputs required, including details of the initial blade geometry. The time of the optimization search depends on the computer capacity and whether the newly obtained design includes airfoil modification or not. In the case of only chord and twist modification, the expected CPU time on the regular work station is approximately 40 minutes. The time required for additional airfoil modification is expected to be in the range of 2.5 hours per investigated desirability weights combination. The volume of the considered blade geometries is estimated on the level of thousands and tens of thousands and is the multiple of the blade elements number. Therefore, the CFD and FEM approaches cannot be applied to replace BEM and other proposed methods in the optimization search but rather as a comparison tool to validate only several obtained geometries.

ACTA UNIVERSITATIS LAPPEENRANTAENSIS

501. MAXIMOV, ALEXANDER. Theoretical analysis and numerical simulation of spectral radiative properties of combustion gases in oxy/air-fired combustion systems. 2012. Diss.
502. KUTVONEN, ANTERO. Strategic external deployment of intellectual assets. 2012. Diss.
503. VÄISÄNEN, VESA. Performance and scalability of isolated DC-DC converter topologies in low voltage, high current applications. 2012. Diss.
504. IKONEN, MIKA. Power cycling lifetime estimation of IGBT power modules based on chip temperature modeling. 2012. Diss.
505. LEIVO, TIMO. Pricing anomalies in the Finnish stock market. 2012. Diss.
506. NISKANEN, ANTTI. Landfill gas management as engineered landfills – Estimation and mitigation of environmental aspects. 2012. Diss.
507. QIU, FENG. Surface transformation hardening of carbon steel with high power fiber laser. 2012. Diss.
508. SMIRNOV, ALEXANDER. AMB system for high-speed motors using automatic commissioning. 2012. Diss.
509. ESKELINEN, HARRI, ed. Advanced approaches to analytical and systematic DFMA analysis. 2013.
510. RYYNÄNEN, HARRI. From network pictures to network insight in solution business – the role of internal communication. 2013. Diss.
511. JÄRVI, KATI. Ecosystem architecture design: endogenous and exogenous structural properties. 2013. Diss.
512. PIILI, HEIDI. Characterisation of laser beam and paper material interaction. 2013. Diss.
513. MONTO, SARI. Towards inter-organizational working capital management. 2013. Diss.
514. PIRINEN, MARKKU. The effects of welding heat input usability of high strength steels in welded structures. 2013. Diss.
515. SARKKINEN, MINNA. Strategic innovation management based on three dimensions diagnosing innovation development needs in a peripheral region. 2013. Diss.
516. MAGLYAS, ANDREY. Overcoming the complexity of software product management. 2013. Diss.
517. MOISIO, SAMI. A soft contact collision method for real-time simulation of triangularized geometries in multibody dynamics. 2013. Diss.
518. IMMONEN, PAULA. Energy efficiency of a diesel-electric mobile working machine. 2013. Diss.

519. ELORANTA, LEENA. Innovation in a non-formal adult education organisation – multi-case study in four education centres. 2013. Diss.
520. ZAKHARCHUK, IVAN. Manifestation of the pairing symmetry in the vortex core structure in iron-based superconductors. 2013. Diss.
521. KÄÄRIÄINEN, MARJA-LEENA. Atomic layer deposited titanium and zinc oxides; structure and doping effects on their photoactivity, photocatalytic activity and bioactivity. 2013. Diss.
522. KURONEN, JUHANI. Jatkuvan äänitehojakautuman algoritmi pitkien käytävien äänikenttien mallintamiseen. 2013. Diss.
523. HÄMÄLÄINEN, HENRY. Identification of some additional loss components in high-power low-voltage permanent magnet generators. 2013. Diss.
524. SÄRKKÄ, HEIKKI. Electro-oxidation treatment of pulp and paper mill circulating waters and wastewaters. 2013. Diss.
525. HEIKKINEN, JANI. Virtual technology and haptic interface solutions for design and control of mobile working machines. 2013. Diss.
526. SOININEN, JUHA. Entrepreneurial orientation in small and medium-sized enterprises during economic crisis. 2013. Diss.
527. JÄPPINEN, EERO. The effects of location, feedstock availability, and supply-chain logistics on the greenhouse gas emissions of forest-biomass energy utilization in Finland. 2013. Diss.
528. SÖDERHOLM, KRISTIINA. Licensing model development for small modular reactors (SMRs) – focusing on the Finnish regulatory framework. 2013. Diss.
529. LAISI, MILLA. Deregulation's impact on the railway freight transport sector's future in the Baltic Sea region. 2013. Diss.
530. VORONIN, SERGEY. Price spike forecasting in a competitive day-ahead energy market. 2013. Diss.
531. PONOMAREV, PAVEL. Tooth-coil permanent magnet synchronous machine design for special applications. 2013. Diss.
532. HIETANEN, TOMI. Magnesium hydroxide-based peroxide bleaching of high-brightness mechanical pulps. 2013. Diss.
533. TYKKÄLÄ, TOMMI M. Real-time image-based RGB-D camera motion tracking and environment mapping. 2013. Diss.
534. PEKKOLA, SANNA. Performance measurement and management in a collaborative network. 2013. Diss.
535. PANOREL, IRIS CHERRY. Pulsed corona discharge as an advanced oxidation process for the degradation of organic compounds in water. 2013. Diss.

536. TORKKELI, LASSE. The influence of network competence of internationalization of SMEs. 2013. Diss.
537. MOLANDER, SOLE. Productivity and services – safety telephone services for the elderly. 2013. Diss.
538. SITARZ, ROBERT. Identification of research trends in the field of separation processes. Application of epidemiological model, citation analysis, text mining, and technical analysis of the financial markets. 2013. Diss.
539. KATTEDEN, KAMIEV. Design and testing of an armature-reaction-compensated permanent magnet synchronous generator for island operation. 2013. Diss.
540. HÄMÄLÄINEN, HARRI. Integration of learning supportive applications to development of e-portfolio construction process. 2013. Diss.
541. RATCHANANUSORN, WARIN. Development of a process for the direct synthesis of hydrogen peroxide in a novel microstructured reactor. 2013. Diss.